THE PENNSYLVANIA STATE UNIVERSITY
SCHREYER HONORS COLLEGE

DEPARTMENT OF MECHANICAL ENGINEERING

Rupture Risk for Intercranial Aneurysms with Varying Inflow Conditions

EVAN LAWLER
SPRING 2023

A thesis
submitted in partial fulfillment
of the requirements
for a baccalaureate degree
in Mechanical Engineering
with honors in Mechanical Engineering

Reviewed and approved* by the following:

Dr. Melissa Brindise
Assistant Professor of Mechanical Engineering
Thesis Supervisor

Dr. Margaret Byron
Assistant Professor of Mechanical Engineering
Honors Adviser

* Electronic approvals are on file.

ABSTRACT

Intracranial aneurysms (IA) are a relatively common abnormality within the blood vessels of the brain that pose a risk for subarachnoid hemorrhage. Evaluating the risk of rupture of these aneurysms is an important clinical challenge. There is a field of study that seeks to connect the hemodynamic characteristics of blood flow within the aneurysm and its risk of rupture. While many studies have compared hemodynamics and risk of rupture, there is little information on how varying inflow conditions impacts these characteristics of interest. This study uses Particle Tracking Velocimetry (PTV) to inspect the fluid mechanical characteristics of flow within an idealized IA at two unique pulsatile frequencies of 180-bpm and 128-bpm. This study will compare these two test cases using inflow concentration, flow complexity, flow impingement zone, flow stability, and wall shear stress as the metrics for evaluation. These hemodynamic characteristics have been shown to be associated with risk of rupture and will be used to evaluate how changing the frequency impacts the risk of rupture.

TABLE OF CONTENTS

LIST OF FIGURES iii

LIST OF TABLES iv

ACKNOWLEDGEMENTS v

Chapter 1 Introduction 1

- Background and Motivation 1
- Modalities used to Investigate IA Hemodynamics 2
- The Role of Hemodynamic Factors 4
- Research Goal and Objective 7

Chapter 2 Experimental Configuration 9

- In Vitro IA Model Manufacturing 9
- Flow Loop Set-Up 10
- Particle Tracking Velocimetry Set-Up 12
- Working Fluids 14
- Experimental Test Cases 15

Chapter 3 Data Processing 17

- PTV Processing 17
- Velocity Filters 18
- Gridding 19
- Data Denoising 19
- Post-Processed Hemodynamic Metrics 20

Chapter 4 Results 21

- Inflow Concentration 21
- Flow Complexity 23
- Flow Impingement Zone 24
- Flow Stability 26
- Wall Shear Stress 27

Chapter 5 Discussion 30

Appendix A 34

LIST OF FIGURES

Figure 1. A flow loop set up schematic with cameras, geometry, pressure transducer, flow meter, reservoir, and gear pump. Adapted from [12]. 3

Figure 2. A normal vessel wall compared to an aneurysm vessel wall. Adapted from [16]. 5

Figure 3. Colorized plot of WSS on geometry....5

Figure 4. Manufacturing the idealized geometry. A) patient scan B) idealized CAD model C) PDMS idealized model. 10

Figure 5. Flow loop configuration A) Reservoir B) Inflow C) Outflow D) Geometry Box E) Flow Meters F) Pressure Transducers. 10

Figure 6. Four cameras are positioned to triangulate particle position within aneurysm. 13

Figure 7. Optical train directing laser beam to aneurysm model. 13

Figure 8. Index matched PDMS and blood analog. 14

Figure 9. Waveform used for 128-bpm case. 15

Figure 10. Waveform used for 180-bpm case. 16

Figure 11. A) 180bpm case B) 128 bpm case; raw velocity data from DaVis. 17

Figure 12. Velocity data visualized in ParaView before implementing velocity thresholds along the x, y, and z directions. 18

Figure 13. Velocity data visualized in ParaView after implementing velocity thresholds along the x, y, and z directions. 18

Figure 14. The velocity gradient cross section maps for A) 180bpm case and B) 128bpm case. 22

Figure 15. Inflow velocity profile 180bpm case. 22

Figure 16. Inflow velocity profile 128bpm case. 23

Figure 17. Swirl strength cross section for A) 180bpm case and B) 128bpm case. 24

Figure 18. Flow impingement velocity profile for 180bpm case. 25

Figure 19. Flow impingement velocity profile for 128bpm case. 25

Figure 20. 180bpm vorticity gradient cross section plot: A) Peak Systole B) Mid Systole C) Peak Diastole D) Mid Diastole. 26

Figure 21. 128bpm vorticity gradient cross section plot: A) Peak Systole B) Mid Systole C) Peak Diastole D) Mid Diastole. 26

Figure 22. Wall shear stress gradient at peak systole A) 180-bpm case B) 128-bpm case.....27

Figure 23. Wall shear stress gradient at peak diastole A) 180-bpm case B) 128-bpm case.....28

Figure 24. Wall shear stress gradient time averaged A) 180-bpm case B) 128-bpm case.....28

ACKNOWLEDGEMENTS

I would like to thank my advisor Dr. Melissa Brindise. Her support and guidance have been crucial in completing this research and thesis. Her wealth of knowledge and expertise in this field have taught me more than I could have ever imagined. Under her guidance, this thesis has been both an incredible and academically enriching experience.

Next, I would like to thank my fellow lab team members: Justin, Abby, Kathryn, Henry, and Baha. Learning and building side by side with them has been a constant help. Their support and collaboration were crucial to the success of this project.

I would like to thank my friends and family whose love and support have kept me motivated not only through my thesis but through all of college. My brothers: Ryan, Jared, Baba, and Conner have been so encouraging and helped me overcome every challenge.

Finally, I would like to specifically thank my mom and dad. They have been as supportive as two parents could ever be and constantly encourage me to pursue my ambitions. I am deeply grateful for their sacrifices and effort to make my entire college experience possible.

Chapter 1
Introduction

Background and Motivation

Intracranial aneurysms (IA) are anormal bulges in blood vessels in the brain that can rupture. Approximately 3% of the global population is estimated to have an unruptured IA (UIA) [1]. The rupture of an IA results in a subarachnoid hemorrhage (SAH), a form of stroke, that can cause permanent brain damage or death and accounts for 10% of all strokes [2]. In hospitalized cases, SAHs have a 18% mortality rate [3]. However, it is estimated that about two-thirds of all UIAs can be considered stable, such that they will not rupture throughout the patient's lifetime [4]. Moreover, treatment of a UIA requires a procedure or surgery of the brain, which carries inherent risk of complication, estimated at 10-14% [5]. Thus, accurate assessment of a UIA's risk of rupture is critical as clinicians aim to avoid performing unnecessary procedures on stable aneurysms, while also appropriately treating aneurysms that will rupture. Unfortunately, the mechanisms that cause an aneurysm to grow and rupture remain largely unknown, making such risk assessments challenging [4].

Current clinical practices of evaluating risk of rupture most often focus on health status, age, familial history, size, and location of the aneurysms as well as certain behavioral risk factors, namely, high blood pressure, smoking, and alcohol abuse [2], [6], [7]. While these factors are important to consider, there is a growing consensus that other hemodynamic and morphological elements of an aneurysm could impact the likelihood of rupture [4]. Hemodynamics refers to the forces and mechanics involved in circulation of blood through tissue and organs in the body. These

factors include wall shear stress (WSS), oscillating shear index (OSI), inflow concentration, flow stability, flow impingement, and flow complexity. Morphological discriminants of an aneurysm are geometric-based elements such as aspect ratio and size of the aneurysm [8]. Better understanding the risks associated with certain morphological and hemodynamic factors as well as their role in influencing IA progression could provide clinicians with more tools to guide their decision making. In fact, updated guidelines were published by the American Heart Association (AHA) and American Stroke Association (ASA) for the management of aneurysmal subarachnoid hemorrhage (aSAH) where hemodynamic and morphological factors were explicitly cited as an important consideration in risk assessment [4].

Modalities used to Investigate IA Hemodynamics

When studying the specific role of hemodynamic factors in IA rupture, past studies have used multiple modalities including computational fluid dynamics (CFD), Particle Tracking Velocimetry (PTV), as well as both *in vivo* and *in vitro* 4D-Flow magnetic resonance imaging (MRI). Each of these techniques seeks to evaluate the movement of blood flow within the aneurysm by making certain assumptions about the characteristics of the geometry and fluid. For example, in CFD, it is often assumed that the flow is laminar, and that blood is Newtonian. Such assumptions inherently limit the methods of study and can yield confounding uncertainties across published works. Nonetheless, CFD, PTV, and 4D-Flow MRI have been shown to be valid methods of accurately representing the fluid mechanics of an aneurysm geometry [9].

4D-Flow MRI is the only modality capable of directly measuring IA hemodynamics in vivo. However, 4D-Flow MRI has consequentially limited spatiotemporal resolution. This can lead to WSS estimates being under-resolved by as much as 40% [10].

PTV is a high precision experimental technique to noninvasively measure fluid flow velocity. Here, we use it to measure flow through a mock circulatory loop designed to create specific flow conditions using a blood analog working fluid. Neutrally buoyant particles are suspended in the fluid and used as flow tracers. The particles are illuminated using a high-power laser and tracked in time using high-speed cameras. Particle displacements between successive image frames can be computed using particle tracking velocimetry (PTV) methods or windowed cross correlations [11]. These particle displacements are proportional to the instantaneous velocity of the fluid and can be used for subsequent analysis and to draw conclusions about the fluid behavior.

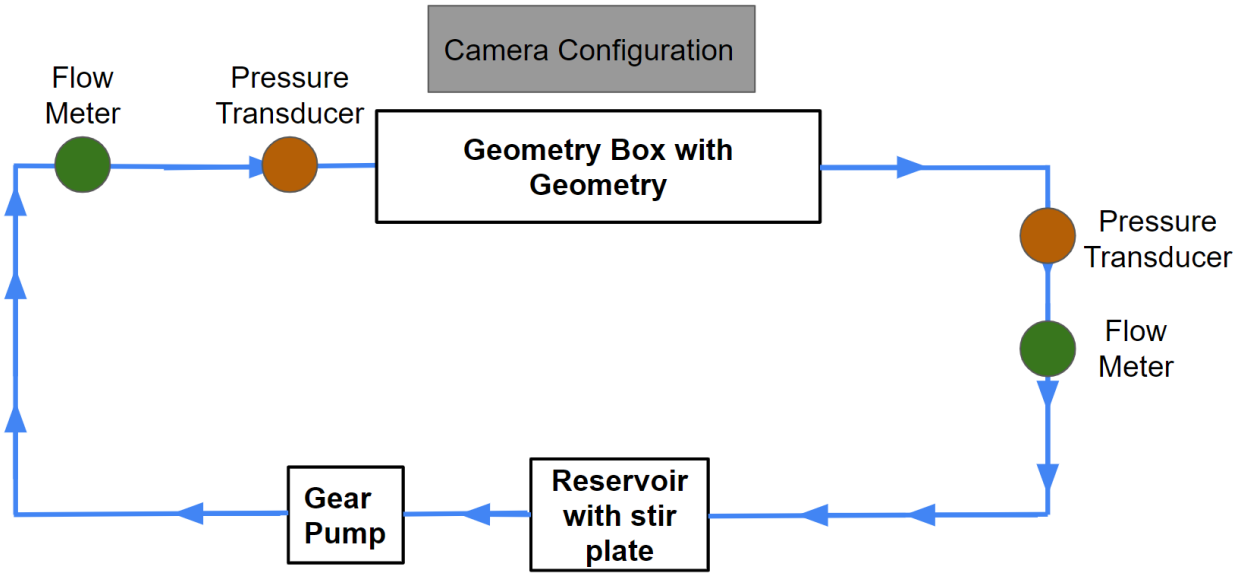

Figure 1. A flow loop set up schematic with cameras, geometry, pressure transducer, flow meter, reservoir, and gear pump. Adapted from [12].

Figure 1 shows a schematic of a typical experimental flow loop for IA studies. Another important aspect of the flow loop is the computer-controlled gear pump. This pump allows for different physiological flow environments to be precisely tested. Adjustments can be made to the flow speed and the frequency of the pulsatile flow.

CFD analysis is a computational approach to modeling fluid flow. This method relies upon the analytical Navier-Stokes equations to model the flow through the aneurysm. CFD has overwhelmingly been the modality of choice in this domain. However, studies have demonstrated that CFD flow fields are highly sensitive to specific simulation parameters such that even small changes in CFD setting can precipitate large changes in the velocity fields [11].

The Role of Hemodynamic Factors

Multiple studies have associated low wall shear stress [WSS] with an increased risk of rupture [13]–[15]. Regions of low WSS are thought to trigger a series of biological indicators that lead to apoptosis, or destruction of, blood vessel cells. This process leads to a thinning and weakening of the blood vessel. Eventually, this process is thought to lead to the rupture of the aneurysms.

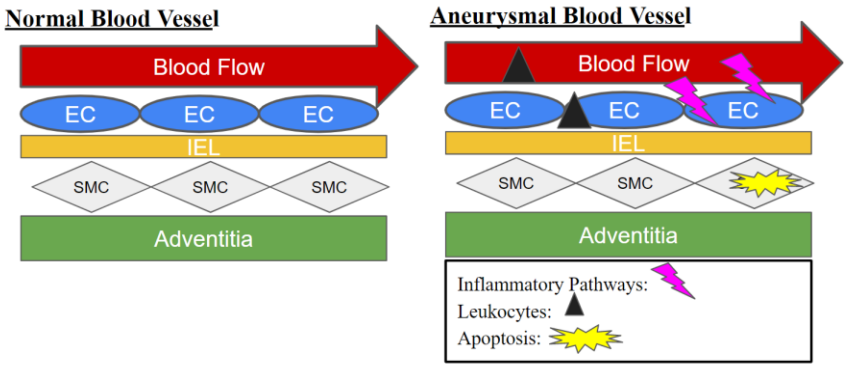

Figure 2. A normal vessel wall compared to an aneurysm vessel wall. Adapted from [16].

Figure 2 compares a normal blood vessel wall with a blood vessel wall in an aneurysm. The biological response to low WSS is exceptionally complex and is beyond the scope of this work; however, the result of this process is apoptosis of cells within the tissue of the blood vessel wall. This process is thought to happen along regions of low WSS and result in the weakening of the blood vessel tissue [16], [17].

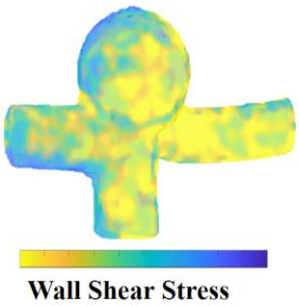

Figure 3. Colorized plot of WSS on geometry.

Figure 3 shows an aneurysm geometry with a color-coded plot of WSS. The regions of blue are associated with the lowest WSS and are therefore considered most likely to rupture [17].

In addition to wall shear stress, there are other hemodynamic factors which have been shown to be correlated to a greater risk of rupture. Firstly, inflow concentration refers to the velocity distribution within the inflow. A concentrated inflow has a small region of high velocity

fluid surrounded by lower velocities, whereas a diffused inflow is more uniform. Additionally, a concentrated inflow has a ‘jet’ of fluid that penetrates relatively deep within the aneurysmal sac [18]–[20]. Concentrated inflow has been shown to be nearly four times more likely to occur in ruptured aneurysms, whereas unruptured aneurysms are more likely to have diffused inflows [18].

Next, flow complexity has also been shown to be correlated a risk of rupture [18], [19]. Flow complexity refers to the number of recirculation zones or vortex structures within the aneurysmal sac. Complex flow patterns are defined as any aneurysm that contains two or more vortex structures or recirculation zones. Complex flow patterns can be used to evaluate the risk of rupture. These complex flow patterns have been shown to occur 4.701 times more often in ruptured aneurysms [18].

Another hemodynamic factor that can be used for evaluating rupture risk is flow impingement zone [19]. This zone refers to the region where the inflow could potentially ‘impact’ the aneurysm wall. These zones have been shown to be correlated to regions of higher wall shear stress. Small impingement regions are three times more likely to occur in ruptured aneurysms [18]

In addition to inflow concentration, flow complexity, and flow impingement zone, flow stability can also be used to evaluate the risk of rupture. Flow stability is a transient factor that refers to the ‘persistence’ of flow patterns during the cardiac cycle. Namely, stable flow patterns are those where the structure of the flow does not change over time. Unstable flow patterns are those where the flow divisions and/or vortex structures are either created or destroyed during the cardiac cycle. Unstable flow patterns have been shown to be 2.7 times more likely to occur in a ruptured aneurysm than an unruptured aneurysm [18].

There are studies that conflict with these results. The role of wall shear stress in aneurysm risk evaluation is particularly disputed and some studies have shown that the higher levels of WSS

are associated with a greater risk of rupture [21]. Due to these conflicting results, concrete conclusions about the role of WSS and other hemodynamic factors related to IA risk of rupture and progression cannot be definitely described. This is a critical factor impacting why hemodynamics have not been integrated into clinical decision making in practice. The presence of these conflicting results suggests that there may be other confounding factors which influence IA progression but have not yet been considered. One such consideration is that aneurysms exist within inherently dynamic systems and experience natural movements, changes in heart rate, and changes in blood speed. These factors could have a large impact on risk of rupture or IA growth but are not presently being considered in studies.

Research Goal and Objective

The current understanding of how WSS is related to the risk of rupture of UIAs has allowed for strong conclusions to be drawn on the increased or decreased risk of rupture [14], [15], [17]. Additionally, it has also been shown that other hemodynamic characteristics such as inflow concentration, flow complexity, flow stability, and flow impingement zone are related to the risk of rupture. However, a critical gap in current knowledge is how specific inflow properties within this dynamic system affect regions of low WSS [8] and other hemodynamic factors [18]. Specifically, pulsation frequency could have a significant impact on the resulting hemodynamic characteristics of an aneurysm and could, consequently, result in an increased risk of rupture. Moreover, different pulsation frequencies within and across patients could be a result of changes in cardiovascular health, diet, glucose levels, stress, or physical exertion. A better understanding of the impact this factor has on the risk of rupture of an IA could be important in shaping clinical

response to patients with IAs. In this work, I present the results from a preliminary PTV experiment investigating the flow through a right middle cerebral artery (R MCA) aneurysm at 128 and 180 bpm and compare those results by examining the presence of WSS and other hemodynamic factors.

Chapter 2
Experimental Configuration

In Vitro IA Model Manufacturing

The R MCA aneurysm model used for this study was based on patient-specific imaging data obtained at Penn State's Hershey Medical Center (HMC) in Hershey, PA. All scan data used in this study was first de-identified by HMC staff. The protocol for this data transfer has been approved by Penn State's Institutional Review Board (IRB). Figure 4a shows the computerized tomography (CT) scan of the R MCA model. The red box highlights the specific location of the aneurysm. From the CT scan, the aneurysm geometry was segmented using the open-source 3D Slicer software, and a CAD model was made as shown in Figure 4b. Although the model was based on patient-specific imaging, modifications to the inflow and outflow vessels were made for ease of PTV imaging. Hence, the model is patient-inspired but considered an idealized geometry. To make the PTV model, the CAD model was 3D printed using polyvinyl alcohol (PVA) filament, which is water dissolvable. The "sacrificial 3D printed model" was then embedded into an acrylic enclosure box and polydimethylsiloxane (PDMS) Sylgard 184 was poured into the box, around the 3D model. PDMS is a semi-transparent silicon elastomer with an index of refraction of 1.4119. Once the PDMS cured, the 3D printed PVA model was dissolved using water and a sonicator. Figure 4c shows the final block model geometry used for this experiment. This model has one inflow vessel (vertical vessel) and two outflow vessels (horizontal vessels).

Figure 4. Manufacturing the idealized geometry. A) patient scan B) idealized CAD model C) PDMS idealized model.

Flow Loop Set-Up

To study the fluid mechanics within an intercranial aneurysm, an experimental flow loop was constructed. The flow loop is meant to mimic many of the important aspects of hemodynamic flow within the body. The flow loop can be described through six main components: the reservoir, inflow, outflow, geometry box, flowmeters, and pressure transducers as shown in Figure 5.

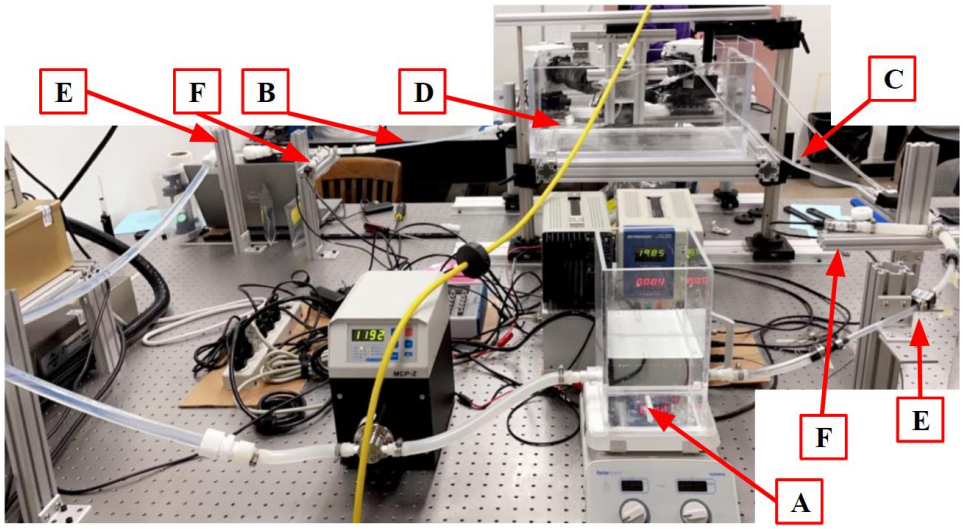

Figure 5. Flow loop configuration A) Reservoir B) Inflow C) Outflow D) Geometry Box E) Flow Meters F) Pressure Transducers.

Firstly, the reservoir is constructed using flat acrylic pieces. The reservoir can be pressurized to modulate the total pressure in the flow loop; however, for experiments herein the reservoir was left open to atmospheric pressure. The reservoir is placed on top of a stir plate to ensure the neutrally buoyant particles remain suspended and well-mixed (avoid clumping) in the fluid. The reservoir houses surplus fluid which helps mitigate the risk of air entering the loop.

Next, the inflow portion of the loop is constructed using ¼" fluorinated ethylene-propylene (FEP) tubing and feeds through the computer-controlled gear pump. FEP tubing was used as it is a rigid tubing which prevents the input pulsatile waveform from being dampened, which can occur if compliant tubing is used. The gear pump used here is an ISMATEC MCP-Z. This pump allows the speed and pulsatile flow frequency of the working fluid to be modulated throughout the entire flow loop by changing the input parameters within a LABVIEW interface.

To ensure the flow environment in the loop matched the expected (designed) flow conditions, flowmeters and pressure transducers were incorporated into the loop both upstream and downstream of the IA model test section. Transonic ME 10 PXL flowmeters were used to measure flow rate, while OMEGA PX309 pressure transducers were used to measure pressure. The flow meter was calibrated by modulating the pump input and collecting the total volume of fluid output by the system for a set period. By measuring the fluid output in that time and the diameter of the tubing, the flow rate could be calculated. The pressure transducers were calibrated by adhering a section of tubing vertically to the wall. The pressure transducer was placed at the bottom and different volumes (heights) of water were added to the tubing. Knowing the density of water, the height of the water in the tube, and the diameter of the tubing, the pressure was calculated. This was compared to the voltage output from the pressure transducer and a calibration constant was found.

Next, fluid travels to a portion of straight unimpeded 1/8” FEP tubing just before the geometry box. This 20” section of tubing ensures that the fluid experiences a section of tubing that is at least 150 diameters in length to create fully developed flow [22]. This section of tubing is roughly 160 diameters and satisfies this requirement. Next, the tubing enters the geometry box. The geometry box is a 20”x7”x8” box created by ¼” acrylic plastic minus the front plate closest to the cameras which is 1/8” acrylic plastic for greater optical resolution. This box contains the surrounding fluid and idealized geometry. After flowing through the geometry, the fluid exits the box through two exit lines on the geometry and is fed back to the reservoir.

Particle Tracking Velocimetry Set-Up

Particle Tracking Velocimetry (PTV) is an experimental technique which uses high-speed imaging to measure the displacement of neutrally buoyant flow tracers, which can be used to calculate flow velocity [23]. Here, we use it to measure the fluid flowing through the aneurysm geometry. In this work, volumetric PTV was used such that particles could be triangulated in 3D space and 3-component (u, v, w) velocity vectors could be resolved. For IAs, volumetric PTV is particularly important as the complex geometries are generally highly three-dimensional. The PTV set-up can be summarized by considering the camera and the laser configurations.

Firstly, the camera configuration is made up of four high-speed 4-megapixel VEO 440 cameras. These cameras are arranged such that they can triangulate the position of the particles along the x, y, and z axes. The figure below shows how these cameras are each positioned to provide a different angle view of the geometry.

Figure 6. Four cameras are positioned to triangulate particle position within aneurysm.

The high-powered laser is a crucial component to the PTV set-up because it illuminates the fluorescent particles passing through the idealized geometry. The laser is a Photonics DM30-527 high pulse energy laser. The beam of the laser passes through an optical train made up of lenses and mirrors which shape the path of the light to pass through the aneurysm as shown in Figure 7. The laser beam is ultimately formed into a laser volume such that it illuminates the entire aneurysm geometry.

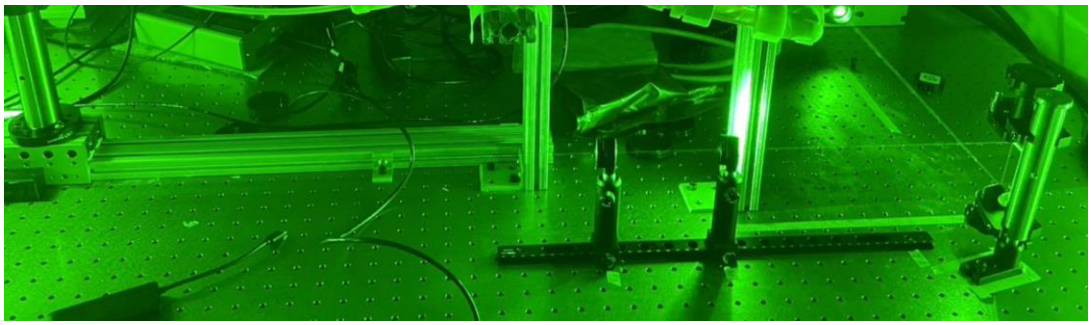

Figure 7. Optical train directing laser beam to aneurysm model.

Working Fluids

This study required the creation of two fluids: the in-line "working" fluid and surrounding fluid. The in-line fluid serves as a blood analog such that it needed to maintain the density and viscosity of blood. This fluid is housed within the flow loop and reservoir and contains the neutrally buoyant particles. The blood-analog working fluid is made up of a mixture of de-ionized (DI) water, glycerol, and urea [24] and the percent composition of these components are 44.1%, 34.5%, and 21.4%, respectively. There are three properties crucial to match the in-line fluid. The measured density and viscosity of the working fluid was $1114\,\frac{\mathrm{kg}}{\mathrm{m}^3}$ and $4.18\text{x}10^{-3}$Pa-s, respectively. A critical aspect for both the working and surrounding fluids was that they maintained the same index of refraction as the PDMS geometry. The index of refraction characterizes how much the light rays change direction when entering the fluid. The PDMS geometry and working fluids need to be indexed matched in order to minimize optical distortions across cameras. The index of refraction for the two fluids was 1.4119 ± 0.0005 which is essentially the same as the PDMS geometry. Figure 8 shows the index matched fluid and material.

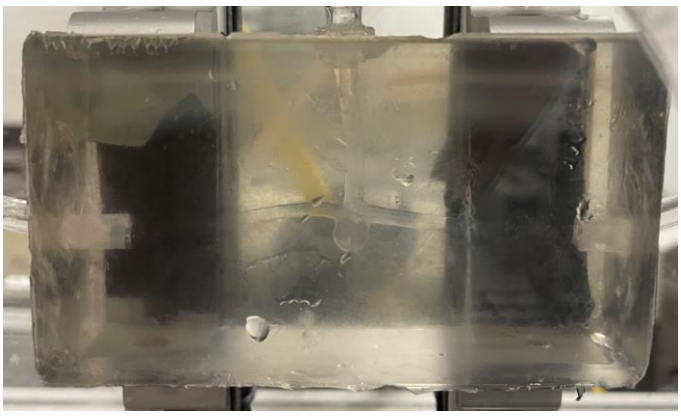

Figure 8. Index matched PDMS and blood analog.

With the materials index matched, the submerged geometry essentially disappears which allows the laser to illuminate only the particles. This makes it possible for the camera to see through the material and image the particles, which is used to map the blood analog itself.

Experimental Test Cases

Two unique pulsatile frequencies were used during this experiment. These waveforms mimic the blood flow behavior of a cardiac cycle. Figure 9 and Figure 10 show the timestep, with a duration of 5 ms, versus flow rate plots for the 128-bpm and 180-bpm pulsatile frequencies respectively.

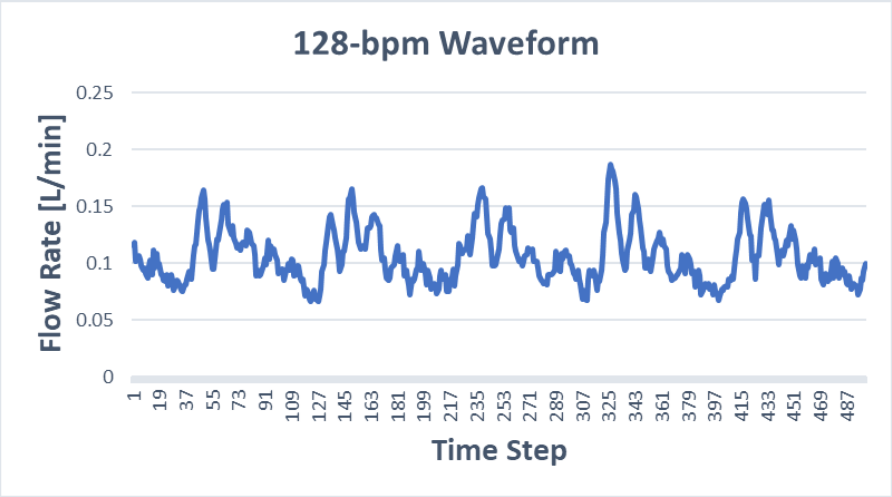

Figure 9. Waveform used for 128-bpm case.

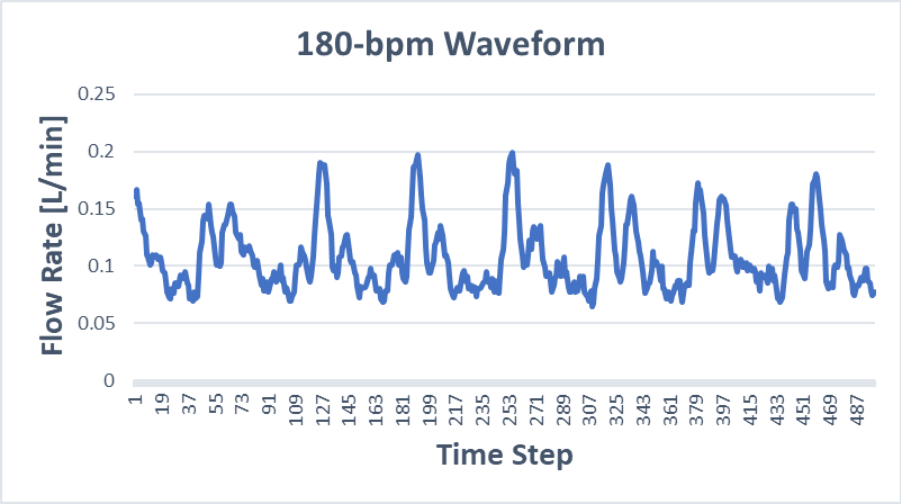

Figure 10. Waveform used for 180-bpm case.

It can be seen from Figures 9 and 10 that the amplitudes of the waveforms are similar, but their pulsatile cycle frequency is not. Figure 9 shows five cardiac cycles whereas Figure 10 shows seven cardiac cycles in the same number of timesteps. Peak systole is the point within the cardiac cycle where the heart is expelling blood and is characterized in these plots by the maximum flow rate peaks seen in both Figures 9 and 10. Peak diastole is where the heart fills with blood and is shown in these plots as the minimum flow rate point of the cardiac cycle.

Chapter 3
Data Processing

PTV Processing

The particle tracks were computed using LaVision's DaVis Shake-the-Box (STB) workflow. Shake-the-box is a method of particle tracking that is designed to include both temporal and spatial information. It is different than other particle tracking velocimetry (PTV) methods because, other than the first several timesteps, it predicts the particle position in subsequent timesteps using the location and velocity of each particle in previous timesteps. This allows for the program to quickly process high particle density three-dimensional data all while capturing a large percentage of true particles and limiting the creation of ghost (falsely triangulated) particles [25].

By compiling the images, the program creates a grouping of velocity vectors. The software produced 12501, 0.3125ms, timesteps. Figure 11 below shows these velocity vectors for each pulsatile frequency at one of the timesteps.

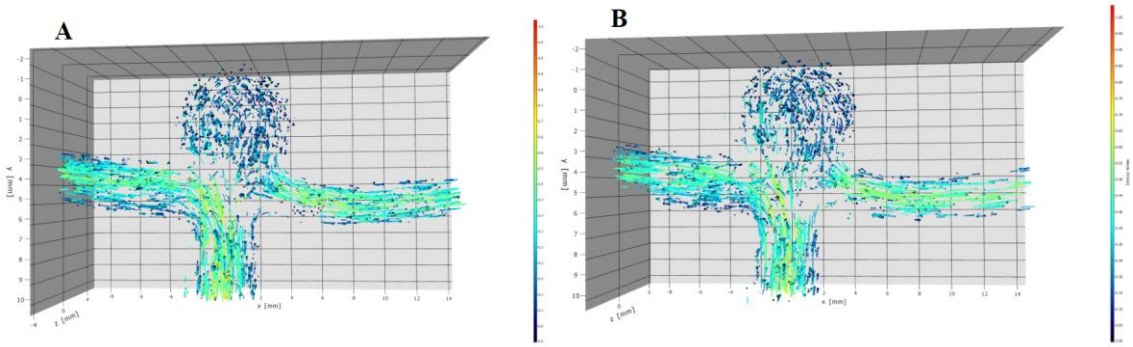

Figure 11. A) 180bpm case B) 128 bpm case; raw velocity data from DaVis.

The data visualized here can be processed within DaVis. The velocity profiles can be gridded to produce plots that allow for conclusions to be drawn about the behavior of the fluid and, by extension, the risk factors surrounding the aneurysm.

Velocity Filters

A challenge surrounding this raw data is that it requires some post processing. Figure 12 visualizes this processing.

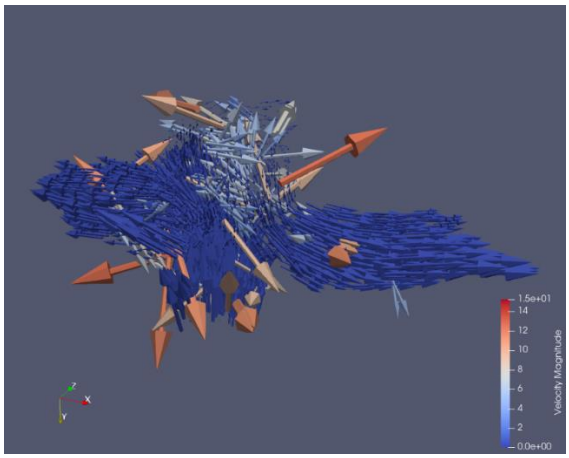

Figure 12. Velocity data visualized in ParaView before implementing velocity thresholds along the x, y, and z directions.

Initially, there are outliers as a result of ghost particles that do not truly represent the behavior of the fluid. These can be seen as the large brown and tan colored vectors. By creating velocity limits in the x, y, and z directions, these outliers can be removed so that the data better characterizes the actual motion. Figure 13 shows how applying these filters removes the outliers.

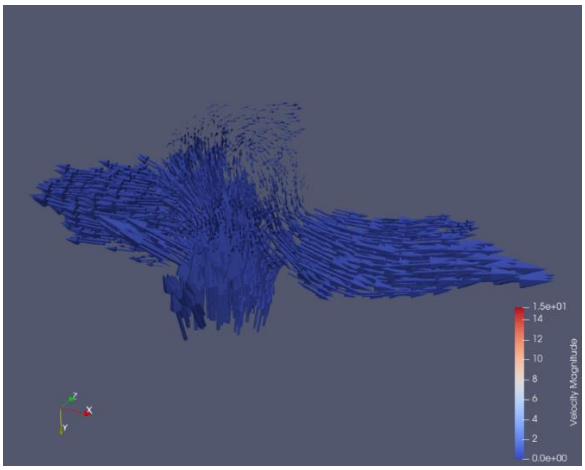

Figure 13. Velocity data visualized in ParaView after implementing velocity thresholds along the x, y, and z directions.

After applying these velocity filters along each component, the data is refined, and outliers are removed. This allows for more accurate conclusions about the flow.

Gridding

Because STB processing was used, the resulting velocity vectors from the PTV processing were on an unstructured grid (Lagrangian). However, to compute WSS and other post processing results, velocity vectors on a structured grid (Eulerian) are needed. To grid the velocity field herein, a weighted average approach was used. This approach is done using a MATLAB code which evaluates a weighted average of velocities at each grid node. Initially, a distance of half the grid length was used to search for particles around the grid node to evaluate the average velocity. This range would increase if less than three particles were found within that range. Once three particles were found, the code would combine their velocities using an inverse-squared radial distance weighted averaging [11].

Data Denoising

The gridded velocity fields were then denoised using proper orthogonal decomposition (POD) which utilized the entropy-line fit (ELF) autonomous thresholding method. The main purpose of POD is to first identify and then remove noise in the data set. Noise occurs in all PTV experiments. It is a consequence of error and uncertainties within the instrumentation and velocity measurements [11], [26]. Removing this noise makes the data more accurate and better represents the actual flow patterns. The efficacy of POD is dictated by the selection of modes which are used

for velocity field reconstruction. The ELF method is an autonomous and highly optimized selection of these modes that allows for highly accurate noise identification [26].

Post-Processed Hemodynamic Metrics

Using the gridded velocity fields, WSS was computed for each test case. WSS was computed by using a thin-plate spline radial basis function (TPS-RBF). This method performs a smoothing and reduces errors. The code computes an inward-facing normal vector at each point on the surface of the aneurysm and maps the velocity coordinate to the equivalent STL surface point. It is a known issue that velocity gradients calculated near the wall have magnitudes that vary based on each specific point's distance from the wall [27]. To mitigate this issue, the WSS calculation was extended beyond this biased region, reducing this variability. This method reduces the near-wall spatial variation to about 5%. Despite this error reducing implementation, all WSS values reported should only be compared relative to values expressed in this report and not to other studies [11]. In addition to WSS at peak systole and diastole, the time averaged WSS (TAWSS) was also calculated where the wall shear stress was integrated across then divided by the time of one pulsatile cycle.

Chapter 4
Results

Multiple hemodynamic characteristics were evaluated throughout this experiment. Specifically, velocity profiles and associated characteristics, velocity gradients, and WSS, were compared across the two test cases (128-bpm and 180-bpm).

Inflow Concentration

The velocity magnitude maps for the 180 and 128 beats per minute (bpm) cases at peak systole (maximum flow rate) are shown in Figure 14. The regions of red and white highlight the regions of greater velocity within the IA geometry. The maximum centerline velocity observed in the 128-bpm case was 0.29 m/s, while the maximum velocity in the 180-bpm case was 0.30 m/s. It is important to note that, as observed in the inflow waveforms (Figure 9 and Figure 10), the inflow flowrate amplitude was not changed between the two bpm cases, only the frequency was modulated. Hence, the fact that the 180-bpm case maintained a 3.4% higher centerline velocity is expected.

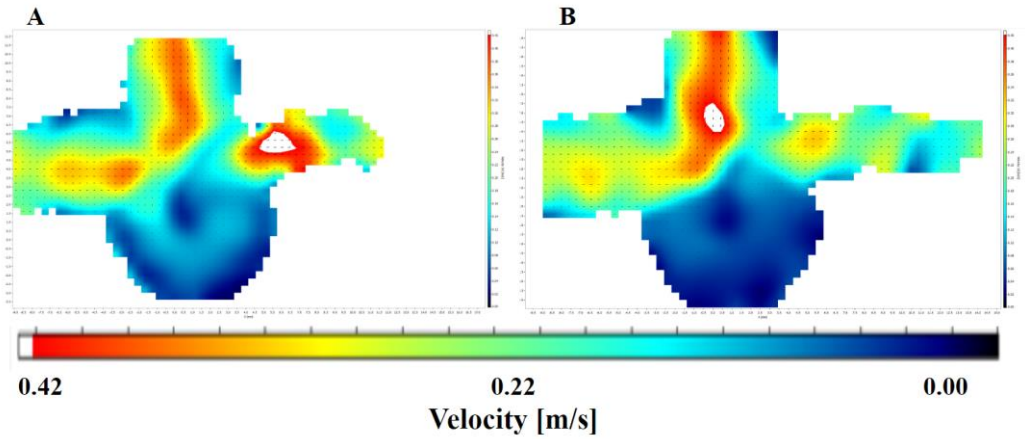

Figure 14. The velocity gradient cross section maps for A) 180bpm case and B) 128bpm case.

From Figure 14, I extracted a velocity profile at a cross section along the inflow region. Figures 15 and 16 show these velocity profiles for the 180 bpm and 128 bpm case respectively.

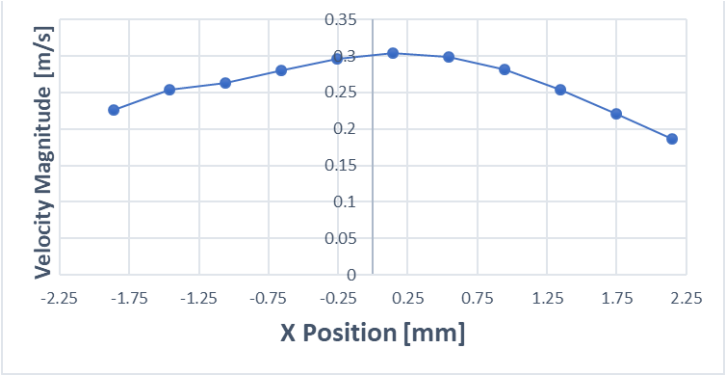

Figure 15. Inflow velocity profile 180bpm case.

Figure 15 illustrates the velocity contour along a cross section of the inflow for the 180 beats per minute case.

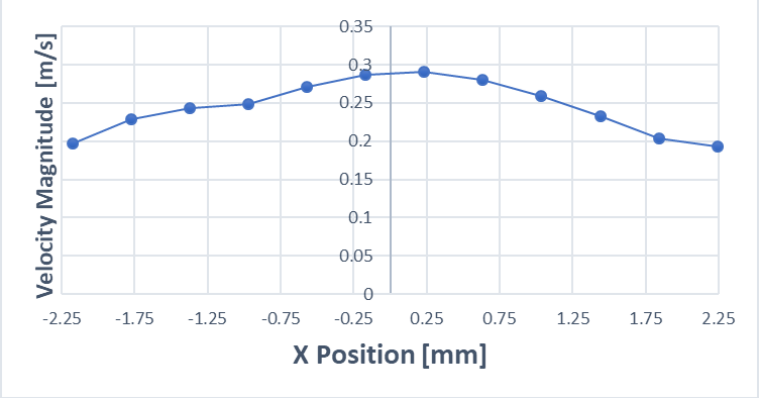

Figure 16. Inflow velocity profile 128bpm case.

Figure 16 plots the velocity profile along an inflow cross section for the 128-bpm case. The data shown in these plots allows for a comparison of how concentrated the 'jet' of fluid is within the 3D shape. To evaluate the size of the velocity stream, a width comparison can be done by summing the distance along the x axis that it takes for the profile to reach 75% of its maximum speed. The 180-bpm case had an inflow width of 3.6mm and the 128-bpm case had a width of 3.4mm. By evaluating the percent difference between the two widths, the 128-bpm case has an inflow velocity profile which is 5.9% more concentrated.

Flow Complexity

Flow complexity refers to the distribution of coherent structures within the aneurysm. Figure 17 visualizes these structures with a cross section gradient of swirl strength. The regions of blue show instances of swirling fluid. The circular zone shown in blue color within the aneurysmal sac is a vortex. Swirl strength is a metric which describes effective vortex indicator in wall turbulence [28].

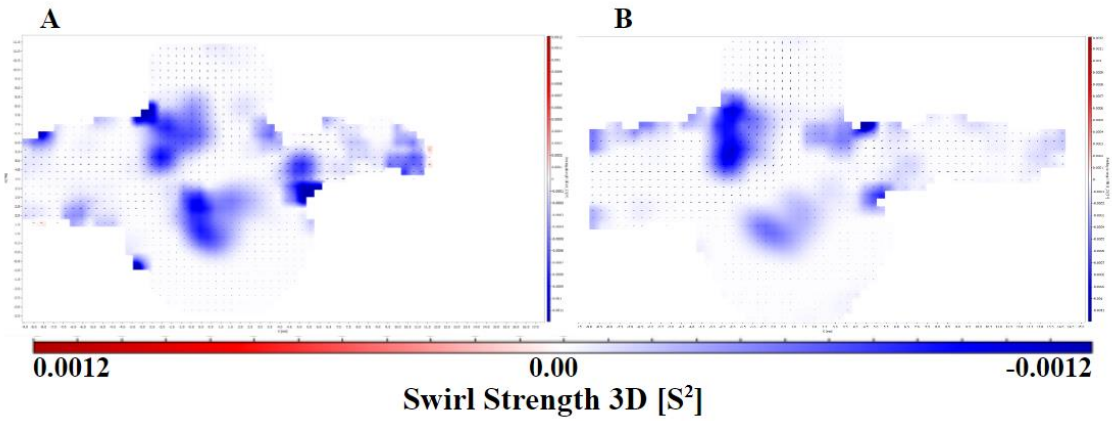

Figure 17. Swirl strength cross section for A) 180bpm case and B) 128bpm case

Between the two pulsatile frequencies, the magnitude of the vortex is stronger in the 180-bpm case. Further, the shape of the vortex within the aneurysmal sac is slightly different between the models with the 180-bpm case showing a longer vortex in the vertical direction, while the 180-bpm case had a larger horizontal directionality of the vortex. The overall number of coherent structures remains the same in both cases.

Flow Impingement Zone

The flow impingement zone is the size of the region within the aneurysmal sac that is being directly impacted by the inflow jet of fluid. To investigate this hemodynamic characteristic, a cross section of velocity data can be plotted along the line intersecting the point where the aneurysm begins to bulge from the blood vessel itself. Figures 18 and 19 plot these profiles for the 180-bpm and 128-bpm case respectively.

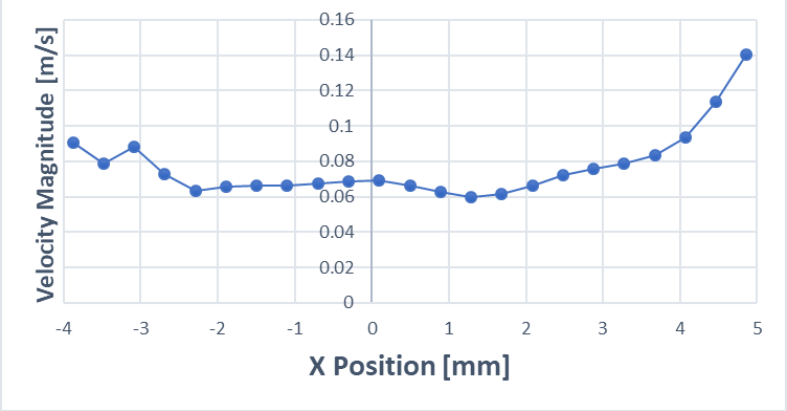

Figure 18. Flow impingement velocity profile for 180bpm case.

Figure 18 visualizes the velocity contour for the 180-bpm case along the line intersecting the aneurysmal sac and the blood vessel.

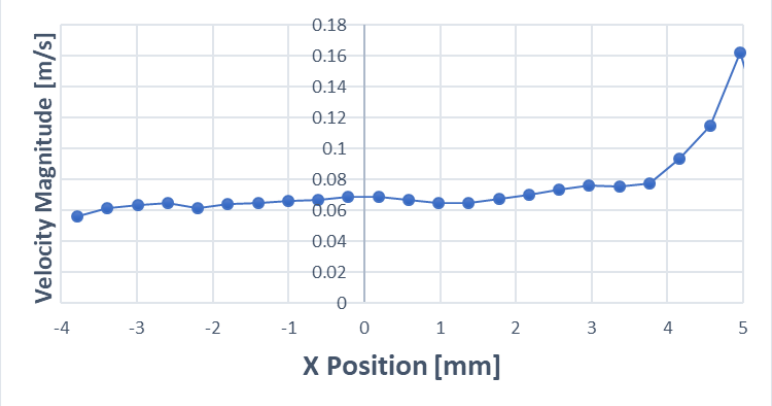

Figure 19. Flow impingement velocity profile for 128bpm case.

Figure 19 plots the points to show the velocity profile for the 128-bpm case. In both cases, it can be seen that along the majority of the cross section no region of the profile stands out as a concentration. This shows that the velocity contour entering the aneurysmal sac is diffused for both pulsatile frequencies. Therefore, there is no identifiable region of flow impingement zone for this aneurysm.

Flow Stability

Flow stability refers to the extent that the coherent structures within the fluid change throughout the cardiac cycle. To examine the coherent structures throughout the cardiac cycle, Figures 20 and 21 show the vorticity gradient plots for the 180-bpm and 128-bpm case at four different times respectively. The four times shown in the plots below are based on the peak systole and diastole points. Peak systole is when the heart is expelling blood and coincides with the maximum blood flow. Peak diastole is when the heart is contacting and coincides with minimum blood flow. The other two points imaged are mid points.

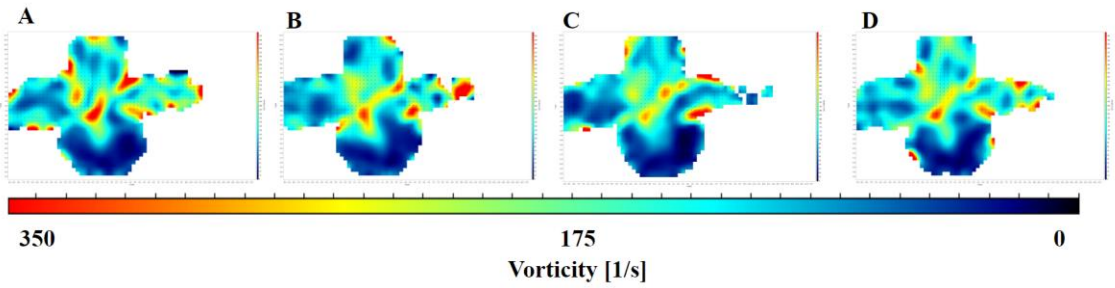

Figure 20. 180bpm vorticity gradient cross section plot: A) Peak Systole B) Mid Systole C) Peak Diastole D) Mid Diastole.

Figure 20 and 21 shows the vorticity gradients for four points along the cardiac cycle. Warmer regions of red and orange coincide with points of higher vorticity.

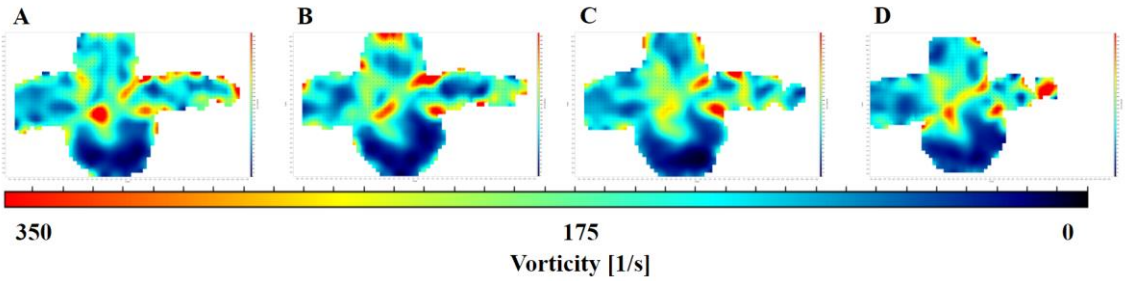

Figure 21. 128bpm vorticity gradient cross section plot: A) Peak Systole B) Mid Systole C) Peak Diastole D) Mid Diastole.

Figure 21 shows the vorticity gradients for the 128-bpm case along four points in the cardiac cycle. By comparing the distribution of vorticity at each point, despite the intensity of the vorticity changes, the coherent structures within the flow stay the same for both pulsatile frequencies.

Wall Shear Stress

Wall shear stress refers to the force per unit area exerted on the vessel wall in the direction tangential to the wall [29]. WSS was calculated along the entire three-dimensional STL of the aneurysm at maximum blood flow and minimum blood flow, peak systole and peak diastole, respectively. Figure 22 shows the comparison of WSS between the 180-bpm and 128-bpm case at peak systole. All WSS figures show the aneurysm in the flipped orientation from previous figures, since this was the direction, they were processed, and the figures were produced. This does not impact the results. The 180-bpm case has greater regions of high WSS compared to the 128-bpm case. Particularly in the aneurysmal sac, Figure 22a contains more regions of high WSS.

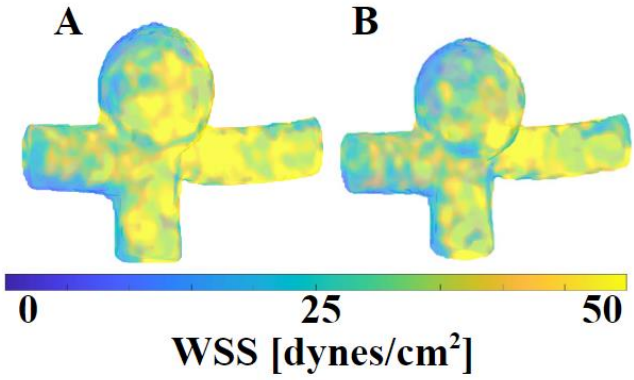

Figure 22. Wall shear stress gradient at peak systole A) 180-bpm case B) 128-bpm case.

Figure 23 compares the two pulsatile frequencies at minimum blood flow, or peak diastole. Compared to the peak systole case, the WSS distributions between cases here are more similar. Both seem to have similar concentrations of high and low WSS both in the aneurysmal sac inflow/outflows.

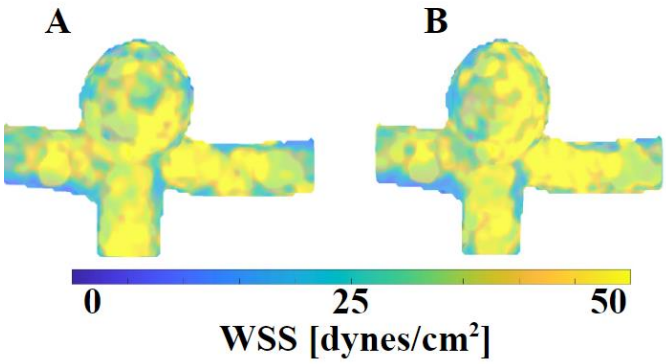

Figure 23. Wall shear stress gradient at peak diastole A) 180-bpm case B) 128-bpm case.

Figure 24 compares the time average WSS (TAWSS) for the 180-bpm and 128-bpm case. This time average is across a whole cardiac cycle and averages the magnitude of WSS. The 180-bpm case has more regions of high WSS within the aneurysm sac. Additionally, it can be seen from the color gradient that the WSS within the 180-bpm case is of greater intensity.

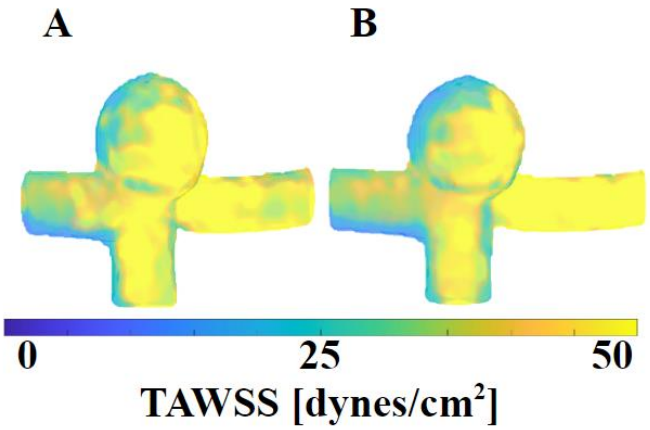

Figure 24. Wall shear stress gradient time averaged A) 180-bpm case B) 128-bpm case.

By comparing the test cases, the 180-bpm case has greater concentration of higher intensity WSS.

Chapter 5
Discussion

The purpose of this experiment was to provide insight into how heart rate potentially impacts the risk of rupture for intercranial aneurysms. This was evaluated by comparing two unique pulsatile frequencies, 128-bpm and 180-bpm, and hemodynamic characteristics which have been shown to be related to risk of rupture. Specifically, those hemodynamic characteristics are: inflow concentration, flow complexity, flow impingement zone, flow stability, and wall shear stress.

Figures 14-16 are related to inflow concentration and compare the two test cases. The data visualized in those figures shows that the 128-bpm case has an inflow that is 5.9% more concentrated than the 180-bpm case. Despite this, the data also revealed that the 180-bpm case had a maximum centerline velocity 3.4% higher than the maximum velocity of the 128-bpm case. This is significant because, as shown in the waveform plots in Figures 9 and 10, the pulsatile frequency was changed but the amplitudes of the waveforms were the same. This shows that the high pulsatile frequency amplified the maximum fluid speed within the geometry. Considering these results, and the fact that previous studies have shown that a more concentrated inflow is more likely to occur in aneurysm that will rupture [18], [21], this hemodynamic characteristic indicates that the 128-bpm case is more likely to rupture than the 180-bpm case.

The next hemodynamic characteristic that could provide insight into the risk of rupture is flow complexity. Figure 17 compares the swirl strength between the two test cases. It can be seen that in each case, there is one coherent structure or vortex within the aneurysmal sac. By comparing the color gradient, the 180-bpm case clearly contains a vortex of much larger magnitude. In fact,

the higher pulsatile frequency case had a maximum swirl strength of almost twice as large as the lower frequency case. Despite this difference in magnitude, flow complexity specifically refers to the number of coherent structures within the flow [18]. Both cases have only one coherent structure within the flow therefore, both cases are simple flow structures. This means that neither is more likely to rupture than the other according to this metric.

The next characteristic to be considered is the flow impingement zone. This characteristic refers to the inflow concentration into the aneurysm and if that inflow force is more localized on a particular portion of the wall of the blood vessel. Figures 18 and 19 show the velocity profiles for a cross section of the flow entering the aneurysm. These profiles show that there is minimal concentration. This indicates that there is not a region within the flow that is applying a large force on the side of the blood vessel wall. This is somewhat expected with the presence of a vortex within the aneurysm. Without a concentration of flow into the aneurysm, this hemodynamic characteristic cannot be evaluated and does not yield significant insight into the risk of rupture between these two test cases.

The next hemodynamic characteristic is flow stability. This refers to the persistence of the coherent structures throughout the cardiac cycle. If the coherent structures change drastically during the cycle, that flow would be unstable. If the coherent structures remain largely the same, this indicates that the flow is more stable. In order to get an accurate understanding of the whole cardiac cycle, four points were selected for comparison—namely, peak systole and peak diastole, as well as two intermediate points. By comparing vorticity plots at these points, it is possible to identify the coherent structures. In both cases, it can be seen in Figures 20 and 21 that coherent structures fade in intensity as they are closer to peak diastole. This is expected since that would be the point of lowest fluid flowrate. Figure 21c is the closest that a coherent structure comes to fully

disappearing. The vortex within the aneurysmal sac in the 128-bpm case becomes very faint at peak diastole. Despite this, the coherent structure can still be identified. In both test cases, throughout the whole cardiac cycle, the coherent structures remain the same. Therefore, both flows could be identified as stable in both cases, meaning that neither is at a high risk of rupture according to this metric [18].

The final parameter evaluated in this study is wall shear stress. While there is some conflicting evidence surrounding the role of wall shear stress in risk assessment, multiple studies have shown that a larger of concentration of low WSS is associated with higher risk of rupture [13]–[15]. Figures 21, 23, and 24 show the distribution of WSS for the two test cases. Figure 23, which evaluated the WSS at peak diastole, was the most inconclusive. The concentrations of WSS looked very similar between 23a and 23b. However, Figure 22 and Figure 24 show a stark difference between the two tests cases. In Figure 22, the 180-bpm case has a much larger concentration of high WSS compared to the 128-bpm case. In Figure 24, the intensity of the WSS and the concentration of regions of high WSS are both far greater for the 180-bpm case. Comparing the two test cases, 128-bpm case has significantly larger regions of low WSS. This indicates that the 128-bpm case may be at a higher risk for aneurysm rupture.

Evaluating the more conclusive hemodynamic characteristics of inflow concentration and WSS, it can be observed that the 128-bpm case likely maintains a larger risk for aneurysm rupture compared to the 180-bpm case. With this conclusion, the pulsatile frequency can be compared to heart rate and it is clear that this right middle cerebral aneurysm is at a greater risk of rupture at the intermediate heart rate as opposed to the high heart rate. This research shows that a patient would be at a higher risk of aneurysm rupture when they are at intermediate heart rate as opposed to high heart rate. This research begins to evaluate one of the parameters of the dynamic system in

which an aneurysm exists and leverages previous conclusions on how hemodynamic factors are related to risk of rupture. However, this evaluation should also be explored against a resting heart rate (i.e., 60 bpm) comparison.

The next possible steps for this research are the testing of more pulsatile frequencies across many different types of aneurysms. In doing so, these conclusions could potentially be extended to different types of aneurysms and possibly reveal more trends relating to heart rate and the risk of aneurysm rupture.

Appendix A

Convert to Grid Code:

```
clear params
%%% SELECT OPTIONS %%%%%%%%%%%%%%%%%%%%%%%%%%%%%%%%%%%%%%%%%%%%%%%%%%%%%%%%%%%%
% Select aneurysm number and file type
params.file.anynum = '001';
params.file.filetype = 'STB';
params.system.cpu = 'lab'; % Can be pc or server
params.file.testcase = '140bpm';
filetype_dt = 1/3200;%0.0015;
% Data import options
params.options.STARTTIME = 1;
params.options.LASTTIME = 12501;
params.options.numtime = 7;
% STL Information
params.stl.stl_save_name = ['STL-ANY-',params.file.anynum];
% Velocity information
params.file.run_num = '1';
if strcmp(params.file.filetype,'STB')
    params.file.basename =
['any',params.file.anynum,'_',params.file.testcase,'_stb_v',params.file.run_num,'_'];
else
    params.file.basename = ['any',params.file.anynum,'_',params.file.filetype,'_'];
end
params.file.velname = [params.file.basename,'regmask_'];
params.file.outvelname = ['any',params.file.anynum,'_stb_v1_','regmask_gridded_'];

%% DIRECTORY AND FILE NAME INFORMATION
% Set directory info based on system
if strcmp(params.system.cpu,'lab')
    params.system.file_base = 'E:\Projects\Cerebral_Aneurysm\Lawler_Data\STB_Data\';
    fslash = '\';
else
    params.system.file_base = '/scratch/shannon/a/mbrindis/Projects/Cerebral_Aneurysm/ANY/';
    fslash = '/';
end
% Directory information
fpath =
[params.system.file_base,params.file.anynum,fslash,params.file.testcase,fslash,'vel_registered_masked',fsl
ash];
savefiles =
[params.system.file_base,params.file.anynum,fslash,params.file.testcase,fslash,'registration_files',fslash
];
savevel =
[params.system.file_base,params.file.anynum,fslash,params.file.testcase,fslash,'vel_gridded',fslash];
savemask =
[params.system.file_base,params.file.anynum,fslash,params.file.testcase,fslash,'registration_files',fslash
,'ANY-',params.file.anynum,'_',params.file.filetype,'_masked_velocity_grid.mat'];

%%% CREATE GRID %%%%%%%%%%%%%%%%%%%%%%%%%%%%%%%%%%%%%%%%%%%%%%%%%%%%%%%%%%%%%%
if strcmp(params.file.filetype,'MRI')
    % Load an MRI velocity file
    fp = load([savevel,params.file.outvelname,num2str(1,'%05i'),'.mat']);
    xmask = unique(fp.x);
    ymask = unique(fp.y);
    zmask = unique(fp.z);
    velmask = nan(length(ymask),length(xmask),length(zmask));
    % Set the velocity mask to zero if a vector is at that location or NaN
    % if no vector is at that location (it is outside the mask)
    for q = 1:1:length(fp.x)
        % Current vector point
```

```
        cx = fp.x(q);
        cy = fp.y(q);
        cz = fp.z(q);
        % Find the mask indices it is closest to
        [~,r_ind] = min(abs(ymask-cy));
        [~,c_ind] = min(abs(xmask-cx));
        [~,z_ind] = min(abs(zmask-cz));
        % Set that mask point to 0
        velmask(r_ind,c_ind,z_ind) = 0;
    end
    % Save the mask grid
    save(savemask,'velmask','xmask','ymask','zmask')
else
    % Grid conversion options
    params.grid.dx = 0.2;
    params.grid.dy = 0.2;
    params.grid.dz = 0.2;

    % Minimum and maximum of X, Y, Z of particles
    params.grid.minX = -9;%15;% -20;%-10; %min(params.data.X);
    params.grid.maxX = 11; %20;%8; %8; %44; %max(params.data.X);
    params.grid.minY = 6;%-6;%-15;%-5;%-8; %-5; %-16; %min(params.data.Y);
    params.grid.maxY = 19;% 24; %22; %15; %30; %max(params.data.Y);
    params.grid.minZ = -5;%-5; %-12;%-7;%-8; %-7; %-14; %min(params.data.Z);
    params.grid.maxZ = 3;%15;%7;%5;%16; %7; %12; %max(params.data.Z);

    % Form x, y, z grid based on minimum and maximum X, Y, Z of particles
    params.grid.x = (params.grid.minX-
0.5*params.grid.dx):params.grid.dx:(params.grid.maxX+params.grid.dx);
    params.grid.y = (params.grid.minY-
0.5*params.grid.dy):params.grid.dy:(params.grid.maxY+params.grid.dy);
    params.grid.z = (params.grid.minZ-
0.5*params.grid.dz):params.grid.dz:(params.grid.maxZ+params.grid.dz);

    % Convert gird to mesh grid and to a linear version of the mesh grid
    [params.grid.X,params.grid.Y,params.grid.Z] = meshgrid(params.grid.x,params.grid.y,params.grid.z);
    params.grid.Xl =
reshape(params.grid.X,[length(params.grid.x)*length(params.grid.y)*length(params.grid.z),1]);
    params.grid.Yl =
reshape(params.grid.Y,[length(params.grid.x)*length(params.grid.y)*length(params.grid.z),1]);
    params.grid.Zl =
reshape(params.grid.Z,[length(params.grid.x)*length(params.grid.y)*length(params.grid.z),1]);

    % Load the STL mask
    params.stl.mask =
load([savefiles,params.stl.stl_save_name,'_',params.file.filetype,'_STLMask_filt.mat']);
    xm = params.stl.mask.stl_x;
    ym = params.stl.mask.stl_y;
    zm = params.stl.mask.stl_z;
    stlmask = params.stl.mask.stlmaskf;

    % Initialize the velocity mask grid
    %velmask = zeros(size(params.grid.Xl));

    % Keep only the grid points that are in the STL mask, NaN the rest
    ubase = zeros(size(params.grid.Xl));
    for q = 1:1:length(ubase)
        % Get the current x,y,z coordiantes
        xcurr = params.grid.Xl(q);
        ycurr = params.grid.Yl(q);
        zcurr = params.grid.Zl(q);

        % Find the mask point that is closest to the grid point
        [~,xind] = min(abs(xm - xcurr));
        [~,yind] = min(abs(ym - ycurr));
        [~,zind] = min(abs(zm - zcurr));
```

```
        % Determine if the current grid point is in the mask
        in_mask = stlmask(yind,xind,zind);

        % Ensure the current point is not larger than the stl mask parameters
        in_x = (xcurr >= min(xm)) & (xcurr <= max(xm));
        in_y = (ycurr >= min(ym)) & (ycurr <= max(ym));
        in_z = (zcurr >= min(zm)) & (zcurr <= max(zm));
        if (in_x == 0) || (in_y == 0) || (in_z == 0)
            in_mask = 0;
        end

        if in_mask == 0
            ubase(q) = NaN;
        end
    end
    % Convert ubase into the velocity mask grid
    velmask = reshape(ubase,[length(params.grid.y),length(params.grid.x),length(params.grid.z)]);
    xmask = params.grid.x;
    ymask = params.grid.y;
    zmask = params.grid.z;
    save(savemask,'velmask','xmask','ymask','zmask')

    % Limit the grid points to only the ones in the mask
    inmask_inds = find(~isnan(ubase));
    params.grid.xm = params.grid.Xl(inmask_inds);
    params.grid.ym = params.grid.Yl(inmask_inds);
    params.grid.zm = params.grid.Zl(inmask_inds);

    %%% READ IN MAT FILE %%%%%%%%%%%%%%%%%%%%%%%%%%%%%%%%%%%%%%%%%%%%%%%%%%%%%%%%%%%%
    time_starts = params.options.STARTTIME:params.options.numtime:params.options.LASTTIME-
params.options.numtime;
    dt = params.options.numtime * filetype_dt;
    for curr_t = 1:1:250 %length(time_starts)
        tic
        curr_act_time = time_starts(curr_t);
        fprintf('\nNow processing %i ...',curr_act_time)
        % Load files for current time step
        curr_t_x = [];
        curr_t_y = [];
        curr_t_z = [];
        curr_t_u = [];
        curr_t_v = [];
        curr_t_w = [];
        t = (curr_t-1)*dt;
        for q = 0:1:params.options.numtime-1
            fp = load([fpath,params.file.velname,num2str(time_starts(curr_t)+q,'%05i'),'.mat']);
            new_x = fp.x; % X is in mm
            new_y = fp.y; % Y is in mm
            new_z = fp.z; % Z is in mm
            new_u = fp.u; % U is in m/s
            new_v = fp.v; % V is in m/s
            new_w = fp.w; % W is in m/s
            % Ensure all vectors are a column vector
            if size(new_x,2)>1, new_x = new_x'; end
            if size(new_y,2)>1, new_y = new_y'; end
            if size(new_z,2)>1, new_z = new_z'; end
            if size(new_u,2)>1, new_u = new_u'; end
            if size(new_v,2)>1, new_v = new_v'; end
            if size(new_w,2)>1, new_w = new_w'; end
            % add the new vectors to the current one
            curr_t_x = [curr_t_x;new_x];
            curr_t_y = [curr_t_y;new_y];
            curr_t_z = [curr_t_z;new_z];
            curr_t_u = [curr_t_u;new_u];
            curr_t_v = [curr_t_v;new_v];
            curr_t_w = [curr_t_w;new_w];
        end
```

```
fprintf(' imported ')

%%% CONVERT TO STRUCTURED GRID %%%%%%%%%%%%%%%%%%%%%%%%%%%%%%%%%%%%%%%%%%%%
% For each grid point, identify particles within an adaptive radius.
% Need minimum of 3 particles. Base radius is half the distance between
% grid points.
% Initialize 3D structure for time step
cu = zeros(size(params.grid.xm));
cv = zeros(size(params.grid.xm));
cw = zeros(size(params.grid.xm));
start_rad = 0.5*params.grid.dx;
if strcmp(params.file.filetype,'CFD')
    max_rad = sqrt(((0.25*params.grid.dx)^2+(0.25*params.grid.dy)^2+(0.25*params.grid.dz)^2));
else
    max_rad = 1e5*start_rad;
end
for p = 1:1:length(params.grid.xm)
    % Obtain x, y, z of current grid points
    cx = params.grid.xm(p);
    cy = params.grid.ym(p);
    cz = params.grid.zm(p);

    % Compute radial distance for all particles in the field
    rad_dist = sqrt((curr_t_x - cx).^2 + (curr_t_y - cy).^2 + (curr_t_z - cz).^2);

    % Find all particles within a radius of 1/2 distance of the grid
    % displacement
    %min_rad_dist(p,1) = min(rad_dist);
    % Find all points within a given radius
    pts_in_rad = (rad_dist <= start_rad); % All points within starting radius
    if sum(pts_in_rad) < 3 || (curr_rad > max_rad)
        % If not enough points in radius, need to adapt radius
        curr_rad = min(rad_dist);
        while sum(pts_in_rad) < 3
            curr_rad = curr_rad + 0.01;
            pts_in_rad = (rad_dist <= curr_rad); % All points within starting radius
        end
    end
    if curr_rad <= max_rad
        % Get velocity and distance for points in radius
        in_rad_u = curr_t_u(pts_in_rad == 1);
        in_rad_v = curr_t_v(pts_in_rad == 1);
        in_rad_w = curr_t_w(pts_in_rad == 1);
        in_rad_dists = rad_dist(pts_in_rad == 1);

        % Compute weight based on square of distance
        dist_wgt = 1./(in_rad_dists.^2);
        dist_wgt = dist_wgt/sum(dist_wgt);

        % Save weighted velocity for point
        cu(p) = sum(in_rad_u.*dist_wgt);
        cv(p) = sum(in_rad_v.*dist_wgt);
        cw(p) = sum(in_rad_w.*dist_wgt);
        rad_save(p) = curr_rad;
    else
        cu(p) = nan;
        cv(p) = nan;
        cw(p) = nan;
    end
end
fprintf('- gridded')
% Keep only indices whose velocities are not NaN values
if curr_t == 1
    kp_inds = ~isnan(cu);
end

% Get the output vectors
```

```
        x = params.grid.xm(kp_inds);
        y = params.grid.ym(kp_inds);
        z = params.grid.zm(kp_inds);
        u = cu(kp_inds);
        v = cv(kp_inds);
        w = cw(kp_inds);

        % Update the velocity mask
        if curr_t == 1
            ubase = zeros(size(params.grid.Xl));
            for q = 1:1:length(ubase)
                % Get the current x,y,z coordiantes
                xcurr = params.grid.Xl(q);
                ycurr = params.grid.Yl(q);
                zcurr = params.grid.Zl(q);

                % Find the mask point that is closest to the grid point
                all_pt_dist = sqrt((x-xcurr).^2 + (y-ycurr).^2 + (z-zcurr).^2);
                pt_dist = min(all_pt_dist);
                close_pt = pt_dist < 0.01;

                % Determine if the current grid point is in the mask
                % Find the mask point that is closest to the grid point
                [~,xind] = min(abs(xm - xcurr));
                [~,yind] = min(abs(ym - ycurr));
                [~,zind] = min(abs(zm - zcurr));
                in_mask = stlmask(yind,xind,zind);

                % Ensure the current point is not larger than the stl mask parameters
                in_x = (xcurr >= min(xm)) & (xcurr <= max(xm));
                in_y = (ycurr >= min(ym)) & (ycurr <= max(ym));
                in_z = (zcurr >= min(zm)) & (zcurr <= max(zm));
                if (in_x == 0) || (in_y == 0) || (in_z == 0)
                    in_mask = 0;
                end
                if close_pt == 0
                    in_mask = 0;
                end
                if in_mask == 0
                    ubase(q) = NaN;
                end
            end
            % Convert ubase into the velocity mask grid
            velmask = reshape(ubase,[length(params.grid.y),length(params.grid.x),length(params.grid.z)]);
            xmask = params.grid.x;
            ymask = params.grid.y;
            zmask = params.grid.z;
            save(savemask,'velmask','xmask','ymask','zmask')
        end

        % Save the grid file in MAT and DAT formats
        % Save mat file

save([savevel,params.file.outvelname,num2str(curr_act_time,'%05i'),'.mat'],'x','y','z','u','v','w','t');

        % Save dat file
        if curr_act_time <= 30
            % Initialize output file
            fid = fopen([savevel,params.file.outvelname,num2str(curr_act_time,'%05i'),'.dat'],'w');
            fprintf(fid,['TITLE = "',params.file.outvelname,num2str(curr_act_time,'%05i'),'"']);
            fprintf(fid,'\r\nVARIABLES = "X", "Y", "Z", "V-X", "V-Y", "V-Z"');

            % Iterate through all points and write only those that are non-zero
            for zz = 1:1:length(x)
                cx = x(zz);
                cy = y(zz);
                cz = z(zz);
```

```
                cu = u(zz);
                cv = v(zz);
                cw = w(zz);
                fprintf(fid,'\r\n%.6f %.6f %.6f %.6f %.6f %.6f',cx,cy,cz,cu,cv,cw);
            end
            % Close dat file
            fclose(fid);
        end
        tval = toc;
        tmin = floor(tval/60);
        tsec = round(tval - tmin*60);
        fprintf(' - completed successfully in %01i:%02i',tmin,tsec)
    end
    fprintf('\n\n')
end
```

Post Processing Code:

```
%% DIRECTORY AND FILE NAME INFORMATION
cadat.FILE.anynum = '001'; % Aneurysm identifiable number
cadat.FILE.filetype = 'STB'; % Should be STB (Shake the box), TOMO, MRI, or CFD
cadat.SYSTEM.cpu = 'lab'; % Can be mac, pc, server, or seagate - changes the directories
appropriately
    % STB loads mat file, TOMO loads dat file
    % MRI loads dat file
% Set orientation information
cadat.options.ORIENT_ON = 1;
cadat.FILE.orientation = '140bpm';
cadat.FILE.orient_short = '140bpm';


%% SET OPTIONS AND CONSTANTS
% Experimental constants
cadat.DATA.rho = 1114; % In kg/m^3
cadat.DATA.mu = 4.18e-3; % In pa-s
cadat.DATA.nu = cadat.DATA.mu/cadat.DATA.rho; % In m^2/s

% Time step options for the current file type
cadat.options.TS = 1; % Start time
cadat.options.Tskip = 7; % Time skip (1 = every one, 2 = every other, etc.) (use 1 for ANY111
and 3 for ANY007)
cadat.options.TE = 12489; %1321; % End time (ANY111 = 1112, ANY007 = 5766)
% Set the time step information for the MRI file type
cadat.options.MRI_TS = 1; % Start time for MRI
cadat.options.MRI_Tskip = 1; % Time skip for MRI
cadat.options.MRI_TE = 20; % End time for MRI (ANY111 = 20, ANY007 = 13)
% Set dt for each time step
if strcmp(cadat.FILE.anynum,'111')
    if cadat.options.ORIENT_ON == 1
        cadat.options.STB_Tskip = 3; % For ANY111=1, for ANY007=3
        cadat.options.dt.mri = 0.0405; % For ANY111=.0405, for ANY007=0.0448
        cadat.options.dt.stb = 1/2000 * cadat.options.STB_Tskip; % For ANY111=1*1/400, for
ANY007=3*1/2000,
        cadat.options.dt.cfd = 0.0015; % For ANY111=0.0015, for ANY007=0.0015
```

```
    else
        cadat.options.STB_Tskip = 5; % For ANY111=1, for ANY007=3
        cadat.options.dt.mri = 0.0405; % For ANY111=.0405, for ANY007=0.0448
        cadat.options.dt.stb = 1/2000 * cadat.options.STB_Tskip; % For ANY111=1*1/400, for
ANY007=3*1/2000,
        cadat.options.dt.cfd = 0.0015; % For ANY111=0.0015, for ANY007=0.0015
    end
elseif strcmp(cadat.FILE.anynum,'001')
    cadat.options.STB_Tskip = 7;
    cadat.options.ct.stb = 1/3200 * cadat.options.STB_Tskip;
else
    cadat.options.STB_Tskip = 3; % For ANY111=1, for ANY007=3
    cadat.options.dt.mri = 0.0448; % For ANY111=.0405, for ANY007=0.0448
    cadat.options.dt.stb = 1/2000 * cadat.options.STB_Tskip; % For ANY111=1*1/400, for
ANY007=3*1/2000,
    cadat.options.dt.cfd = 0.0015; % For ANY111=0.0015, for ANY007=0.0015
end

% Results and computation options
% Velocity smoothing and data set options
cadat.options.RUNPOD = 0; % Run POD on velocity fields (should use gridded, masked, and
registered fields as input)
    cadat.options.USEPOD = 1; % Use the POD filtered velocity fields for all subsequent
calculations
cadat.options.RUNUOD = 0; % Run UOD on velocity fields (should use POD filtered fields as
input)
    cadat.options.USEUOD = 0; % Use the UOD filtered velocity fields for all subsequent
calculations
cadat.options.RUNPHASEAVGSTB = 0; % Run phase averaging on the velocity fields (only needed
for the PTV data)
    cadat.options.USEMRIVEL = 0; % Align the phase averaged velocity to the MRI velocity array
(only use if using 4D flow MRI data)
    cadat.options.USEPHASEAVG = 0; % Use phase averaging for all subsequent calculations
cadat.options.RUNVOXAVG = 0; % Run "voxel averaging" for STB/CFD data for velocity comparisons
to MRI
    cadat.options.USEVOXAVG = 0; % Use the voxel averaged velocity fields for all subsequent
calculation
                                 % Voxel averaging should *ONLY* be used for velocity
comparsion,
                                 % NOT wss, osi rrt, pressure, coherent structures, etc.
cadat.options.CONVERT3DGRID = 0; % Converts the grid to 3D for paraview plotting

% Velocity and flow rate comparisons and calculations
cadat.options.SAVE_VEL_STL_PLOT = 0; % Save the STL plot needed for plotting the WSS
cadat.options.COMPFLOWRATE = 0; % Compute the flow rate for the current modality
    cadat.options.SETXSECS = 0; % The cross sections can be loaded or computed
% Secondary flow variable (i.e. wss, pressure, etc.) calculations
cadat.options.COMPNORMS = 0; % Compute the wall normal vectors for WSS
    cadat.options.SMOOTHNORMS = 1; % Smooth the normals previously computed
    cadat.options.LOADNORMS = 1; % Load in pre-computed velocity normals
    cadat.options.PLOTNORMS = 1; % Plot the loaded velocity normals
cadat.options.COMPVELGRAD = 0; % Compute velocity gradients
cadat.options.COMPDIVERGENCE = 0; % Compute divergence (requires gradients to have been
computed already)
cadat.options.COMPWSS = 0; % Compute wall shear stress (requires gradients to have been
computed already)
cadat.options.COMPOSI = 0; % Compute oscillatory shear index (requires WSS to have already
been computed)
cadat.options.COMPRRT = 0; % Compute relative residence times (requires WSS,OSI to have
already been computed)
```

```
cadat.options.COMPVORT = 0; % Compute vorticity (requires gradients to have been computed
already)
cadat.options.IDCOHERSTRUCT = 0; % Identify coherent structures
cadat.options.TURBANALYSIS = 0; % Compute the turbulent information
    cadat.options.COMPFLUCVEL = 0; % Compute the fluctuating velocities
        cadat.options.LOADALLTIMEFLUCVEL = 0; % Loads all time step fluctuating velocities
(needed for TKE/TI calc)
    cadat.options.COMPFLUCPRESSURE = 0; % Compute the fluctuating pressure
    cadat.options.COMPTURBINT = 0; % Compute the turbulence intensity and TKE
    cadat.options.COMPRESTRESS = 0; % Compute the Reynolds stresses
    cadat.options.COMPFLUCDERIVS = 0; % Compute derivatives of fluctuating velocities
    cadat.options.COMPPRODUCTION = 0; % Compute turbulence production
    cadat.options.COMPPRESSUREDIFF = 0; % Compute turbulence pressure diffusion
    cadat.options.COMPDISSIPATION = 0; % Compute turbulent dissipation rate
    cadat.options.COMPDISSRATETIME = 0; % Compute the dissipation rate in time
    cadat.options.COMPWHTF = 0; % Compute the WHTF of the fluctuating velocites
cadat.options.FILTERPRESSUREFIELD = 0; % Compute pressure
cadat.options.COMPPWV = 0; % Compute the pressure wave velocity
% Save output options
cadat.options.SAVEOUTPUTS = 1; % Choose whether to save the outputs or only compute them

% Plotting options
cadat.options.PLOTSTREAMTRACES = 0;
cadat.options.PLOTVELCOMP = 0;
cadat.options.PLOTVELPROFILES = 0;
cadat.options.PLOTPODMODES = 0;
cadat.options.PLOTVELFIELD = 0;
cadat.options.PLOTCONDVEL = 0;
cadat.options.PLOTVORTFIELD = 0;
cadat.options.PLOTPRESSURE = 0;
cadat.options.PLOTDIVERGENCE = 0;
cadat.options.PLOTWSS = 1;
cadat.options.PLOTWSSXYZ = 1;
cadat.options.PLOTTURBVORTLINE = 1;
cadat.options.PLOTTURBTIMESERIES = 0;
cadat.options.EVALRESTRESS = 0;
cadat.options.PLOTGENMETRIC = 1;
    cadat.options.metric = 'vorticity';
    cadat.options.metric_name = 'vort';
cadat.options.PLOTCS = 0;

% Debug plotting option
cadat.options.DEBUGPLOTS = 1;

%%%%%%%%%%%%%%%%%%%%%%%%%%%%%%%%%%%%%%%%%%%%%%%%%%%%%%%%%%%%%%%%%%%%%%%%%%%%%%%
%%%%%%%%%%%%%%%%%%%%%%%%%%%%%%%%%%%%%%%%%%%%%%%%%%%%%%%%%%%%%%%%%%%%%%%%%%%%%%%
%%% END OF USER INPUTS %%%%%%%%%%%%%%%%%%%%%%%%%%%%%%%%%%%%%%%%%%%%%%%%%%%%%%%%
%%%%%%%%%%%%%%%%%%%%%%%%%%%%%%%%%%%%%%%%%%%%%%%%%%%%%%%%%%%%%%%%%%%%%%%%%%%%%%%
%%%%%%%%%%%%%%%%%%%%%%%%%%%%%%%%%%%%%%%%%%%%%%%%%%%%%%%%%%%%%%%%%%%%%%%%%%%%%%%
%% Set the use/run controls based on the chosen modality
if strcmp(cadat.FILE.filetype,'MRI')
    cadat.options.USEUOD = 0;
    cadat.options.USEPOD = 0;
    cadat.options.USEVOXAVG = 0;
    cadat.options.USEPHASEAVG = 0;
elseif strcmp(cadat.FILE.filetype,'CFD')
    cadat.options.USEUOD = 0;
    cadat.options.USEPOD = 0;
    cadat.options.USEPHASEAVG = 0;
end
```

```
%% Set the directory and file names based on user inputs
% Set the base directory name and slash based on the system being used
if cadat.options.ORIENT_ON
    if strcmp(cadat.SYSTEM.cpu,'lab')
        cadat.DIR.dirbase = 'E:\Projects\Cerebral_Aneurysm\Lawler_Data\STB_Data\'; %Editied
Evan
        fslash = '\';
        addpath 'E:\Projects\Cerebral_Aneurysm\Codes\General-Codes'
        addpath 'E:\Projects\Cerebral_Aneurysm\Codes\General-Codes\decompositions'
        addpath 'E:\Projects\Cerebral_Aneurysm\Codes\General-Codes\multipurpose'
        addpath 'E:\Projects\Cerebral_Aneurysm\Codes\General-Codes\gradients'
    elseif strcmp(cadat.SYSTEM.cpu,'server')
        cadat.DIR.dirbase =
'/scratch/shannon/a/mbrindis/Projects/Cerebral_Aneurysm/ANY/Orientation/';
        fslash = '/';
    elseif strcmp(cadat.SYSTEM.cpu,'seagate')
        cadat.DIR.dirbase = '/Volumes/SEAGATE/CerebralAneurysm/ANY/Orientation/';
        fslash = '/';
        addpath /Users/Melissa/Documents/Code/general_codes/multipurpose
        addpath /Users/Melissa/Documents/Code/general_codes/gradients
        addpath /Users/Melissa/Documents/Code/general_codes/turbulence
        addpath /Users/Melissa/Documents/Code/general_codes/decompositions
    else
        cadat.DIR.dirbase = '/Users/Melissa/Desktop/ANY/Orientation/';
        fslash = '/';
        addpath /Users/Melissa/Documents/Code/general_codes/multipurpose
        addpath /Users/Melissa/Documents/Code/general_codes/gradients
        addpath /Users/Melissa/Documents/Code/general_codes/turbulence
        addpath /Users/Melissa/Documents/Code/general_codes/decompositions
    end
else
    if strcmp(cadat.SYSTEM.cpu,'pc')
        cadat.DIR.dirbase = 'Z:\Projects\Cerebral_Aneurysm\ANY\';
        fslash = '\';
    elseif strcmp(cadat.SYSTEM.cpu,'server')
        cadat.DIR.dirbase = '/home/shannon/a/mbrindis/Projects/Cerebral_Aneurysm/ANY/';
        fslash = '/';
    else
        cadat.DIR.dirbase = '/Users/Melissa/Desktop/ANY/';
        fslash = '/';
        addpath /Users/Melissa/Documents/Code/general_codes/multipurpose
        addpath /Users/Melissa/Documents/Code/general_codes/gradients
    end
end

% Set information based on the file type being used
if strcmp(cadat.FILE.filetype,'STB')
    if cadat.options.ORIENT_ON % Orientation is only for STB
        cadat.DIR.velfiles =
[cadat.DIR.dirbase,cadat.FILE.anynum,fslash,cadat.FILE.orientation,fslash,'vel_gridded',fslash
]; %Evan Editied
        cadat.FILE.basename = ['any',cadat.FILE.anynum,'_stb_v1_regmask_gridded_']; %THIS ONE
        cadat.FILE.podname =
['any',cadat.FILE.anynum,'_',cadat.FILE.orient_short,'_',cadat.FILE.filetype,'_v1_p1_pod_'];
        cadat.FILE.uodname =
['any',cadat.FILE.anynum,'_',cadat.FILE.orient_short,'_',cadat.FILE.filetype,'_v1_p2_uod_'];
        cadat.FILE.paname =
['any',cadat.FILE.anynum,'_',cadat.FILE.orient_short,'_',cadat.FILE.filetype,'_v1_p2s1_phaseav
g_'];
```

```
        cadat.FILE.voxavgname =
['any',cadat.FILE.anynum,'_',cadat.FILE.orient_short,'_',cadat.FILE.filetype,'_v1_p3_voxavg_']
;
    else
        cadat.DIR.velfiles =
[cadat.DIR.dirbase,cadat.FILE.anynum,fslash,cadat.FILE.filetype,fslash,'vel_gridded',fslash];
        cadat.FILE.basename = ['any',cadat.FILE.anynum,'_stb_v1_regmask_gridded_'];
        cadat.FILE.podname = ['any',cadat.FILE.anynum,'_',cadat.FILE.filetype,'_v1_p1_pod_'];
        cadat.FILE.uodname = ['any',cadat.FILE.anynum,'_',cadat.FILE.filetype,'_v1_p2_uod_'];
        cadat.FILE.paname =
['any',cadat.FILE.anynum,'_',cadat.FILE.filetype,'_v1_p2s1_phaseavg_'];
        cadat.FILE.voxavgname =
['any',cadat.FILE.anynum,'_',cadat.FILE.filetype,'_v1_p3_voxavg_'];
    end
elseif (strcmp(cadat.FILE.filetype,'MRI') || strcmp(cadat.FILE.filetype,'MRI_dv') ||
strcmp(cadat.FILE.filetype,'MRI_hv'))
    if strcmp(cadat.FILE.anynum,'007')
        cadat.DIR.velfiles =
[cadat.DIR.dirbase,cadat.FILE.anynum,fslash,cadat.FILE.filetype,fslash,'vel_gridded',fslash];
        cadat.FILE.basename =
['any',cadat.FILE.anynum,'_',cadat.FILE.filetype,'_regmask_gridded_'];
    else
        cadat.DIR.velfiles =
[cadat.DIR.dirbase,cadat.FILE.anynum,fslash,cadat.FILE.filetype,fslash,'vel_registered_masked'
,fslash];
        cadat.FILE.basename = ['any',cadat.FILE.anynum,'_',cadat.FILE.filetype,'_regmask_'];
    end
else
    cadat.DIR.velfiles =
[cadat.DIR.dirbase,cadat.FILE.anynum,fslash,cadat.FILE.filetype,fslash,'vel_gridded',fslash];
    cadat.FILE.basename =
['any',cadat.FILE.anynum,'_',cadat.FILE.filetype,'_regmask_gridded_'];
    cadat.FILE.podname = ['any',cadat.FILE.anynum,'_',cadat.FILE.filetype,'_p1_pod_'];
    cadat.FILE.uodname = ['any',cadat.FILE.anynum,'_',cadat.FILE.filetype,'_p2_uod_'];
    cadat.FILE.voxavgname = ['any',cadat.FILE.anynum,'_',cadat.FILE.filetype,'_p3_voxavg_'];
end

if cadat.options.ORIENT_ON
    cadat.FILE.grid3Dname =
['any',cadat.FILE.anynum,'_',cadat.FILE.orient_short,'_',cadat.FILE.filetype,'_vA_grid3D_'];
    cadat.DIR.podfiles =
[cadat.DIR.dirbase,cadat.FILE.anynum,fslash,cadat.FILE.orientation,fslash,'vel_p1_pod',fslash]
;% Edited Evan
    cadat.DIR.uodfiles =
[cadat.DIR.dirbase,cadat.FILE.anynum,fslash,cadat.FILE.orientation,fslash,'vel_p2_uod',fslash]
;% Edited Evan
    cadat.DIR.pafiles =
[cadat.DIR.dirbase,cadat.FILE.anynum,fslash,cadat.FILE.orientation,fslash,cadat.FILE.filetype,
fslash,'vel_p2s1_phaseavg',fslash];
    cadat.DIR.voxavgfiles =
[cadat.DIR.dirbase,cadat.FILE.anynum,fslash,cadat.FILE.orientation,fslash,cadat.FILE.filetype,
fslash,'vel_p3_voxavg',fslash];
    cadat.DIR.grid3Dfiles =
[cadat.DIR.dirbase,cadat.FILE.anynum,fslash,cadat.FILE.orientation,fslash,cadat.FILE.filetype,
fslash,'vel_pA_grid3D',fslash];
    cadat.DIR.stlfiles =
[cadat.DIR.dirbase,cadat.FILE.anynum,fslash,cadat.FILE.orientation,fslash,'geometry',fslash];
    cadat.DIR.savefiles =
[cadat.DIR.dirbase,cadat.FILE.anynum,fslash,cadat.FILE.orientation,fslash,'registration_files'
,fslash];
```

```
    cadat.DIR.savefiles_horiz =
[cadat.DIR.dirbase,cadat.FILE.anynum,fslash,cadat.FILE.orientation,fslash,'registration_files'
,fslash];
    cadat.DIR.savefiles_vert =
[cadat.DIR.dirbase,cadat.FILE.anynum,fslash,cadat.FILE.orientation,fslash,'registration_files'
,fslash];
    cadat.DIR.saveppfiles =
[cadat.DIR.dirbase,cadat.FILE.anynum,fslash,cadat.FILE.orientation,fslash,'postprocessing_file
s',fslash];
    cadat.DIR.saveppfiles_horiz =
[cadat.DIR.dirbase,cadat.FILE.anynum,fslash,'Horizontal',fslash,'postprocessing_files',fslash]
;
    cadat.DIR.saveppfiles_vert =
[cadat.DIR.dirbase,cadat.FILE.anynum,fslash,'Vertical',fslash,'postprocessing_files',fslash];
    cadat.DIR.saveplots = [cadat.DIR.dirbase,cadat.FILE.anynum,fslash,'plots',fslash];
    cadat.FILE.anyname =
['any',cadat.FILE.anynum,'_',cadat.FILE.orient_short,'_',cadat.FILE.filetype,'_'];
    cadat.FILE.maskgrid = ['ANY-
',cadat.FILE.anynum,'_',cadat.FILE.filetype,'_masked_velocity_grid'];
    cadat.FILE.stlmaskname = ['STL-ANY-
',cadat.FILE.anynum,'_',cadat.FILE.filetype,'_STLMask_filt'];
else
    cadat.FILE.grid3Dname = ['any',cadat.FILE.anynum,'_',cadat.FILE.filetype,'_vA_grid3D_'];
    cadat.DIR.podfiles =
[cadat.DIR.dirbase,cadat.FILE.anynum,fslash,cadat.FILE.orientation,fslash,'vel_p1_pod',fslash]
; % Edited Evan
    cadat.DIR.uodfiles =
[cadat.DIR.dirbase,cadat.FILE.anynum,fslash,cadat.FILE.orientation,fslash,'vel_p2_uod',fslash]
; % Edited Evan
    cadat.DIR.pafiles =
[cadat.DIR.dirbase,cadat.FILE.anynum,fslash,cadat.FILE.filetype,fslash,'vel_p2s1_phaseavg',fsl
ash];
    cadat.DIR.voxavgfiles =
[cadat.DIR.dirbase,cadat.FILE.anynum,fslash,cadat.FILE.filetype,fslash,'vel_p3_voxavg',fslash]
;
    cadat.DIR.grid3Dfiles =
[cadat.DIR.dirbase,cadat.FILE.anynum,fslash,cadat.FILE.filetype,fslash,'vel_pA_grid3D',fslash]
;
    cadat.DIR.stlfiles = [cadat.DIR.dirbase,cadat.FILE.anynum,fslash,'geometry',fslash];
    cadat.DIR.savefiles =
[cadat.DIR.dirbase,cadat.FILE.anynum,fslash,'registration_files',fslash];
    cadat.DIR.saveppfiles =
[cadat.DIR.dirbase,cadat.FILE.anynum,fslash,'postprocessing_files',fslash];
    cadat.DIR.saveplots = [cadat.DIR.dirbase,cadat.FILE.anynum,fslash,'plots',fslash];
    cadat.FILE.anyname = ['any',cadat.FILE.anynum,'_',cadat.FILE.filetype,'_'];
    cadat.FILE.maskgrid = ['ANY-
',cadat.FILE.anynum,'_',cadat.FILE.filetype,'_masked_velocity_grid'];
    cadat.FILE.stlmaskname = ['STL-ANY-
',cadat.FILE.anynum,'_',cadat.FILE.filetype,'_STLMask_filt'];
end


%% INITIAL CALCULATION
% Load the grid mask for the velocity field
% This step is needed for several subsequent processes
fp = load([cadat.DIR.savefiles,cadat.FILE.maskgrid,'.mat']);
velmask = fp.velmask; % Velocity grid mask
maskX = fp.xmask;
maskY = fp.ymask;
maskZ = fp.zmask;
```

```
[Vx,Vy,Vz] = meshgrid(maskX,maskY,maskZ);
dx = maskX(2) - maskX(1); % In mm
dy = maskY(2) - maskY(1); % In mm
dz = maskZ(2) - maskZ(1); % In mm
cadat.DATA.X = Vx;
cadat.DATA.Y = Vy;
cadat.DATA.Z = Vz;

% Load the STL mask  - needed for computing flow rate
fp = load([cadat.DIR.savefiles,cadat.FILE.stlmaskname,'.mat']);
cadat.STL.maskf = fp.stlmaskf;
cadat.STL.maskf(cadat.STL.maskf == 0) = NaN;
cadat.STL.x = fp.stl_x;
cadat.STL.y = fp.stl_y;
cadat.STL.z = fp.stl_z;
unqX = unique(cadat.STL.x);
cadat.STL.dx = unqX(2)-unqX(1);
unqY = unique(cadat.STL.y);
cadat.STL.dy = unqY(2)-unqY(1);
unqZ = unique(cadat.STL.z);
cadat.STL.dz = unqZ(2)-unqZ(1);

%%%%%%%%%%%%%%%%%%%%%%%%%%%%%%%%%%%%%%%%%%%%%%%%%%%%%%%%%%%%%%%%%%%%%%%%%%%%%%%
%%%%%%%%%%%%%%%%%%%%%%%%%%%%%%%%%%%%%%%%%%%%%%%%%%%%%%%%%%%%%%%%%%%%%%%%%%%%%%%
%%% VELOCITY FILTERING OPERATIONS %%%%%%%%%%%%%%%%%%%%%%%%%%%%%%%%%%%%%%%%%%%%%%
%%%%%%%%%%%%%%%%%%%%%%%%%%%%%%%%%%%%%%%%%%%%%%%%%%%%%%%%%%%%%%%%%%%%%%%%%%%%%%%
%%%%%%%%%%%%%%%%%%%%%%%%%%%%%%%%%%%%%%%%%%%%%%%%%%%%%%%%%%%%%%%%%%%%%%%%%%%%%%%

%% PROPER ORTHOGONAL DECOMPOSITION SMOOTHING
% This step smooths the data using POD in 3D. If POD is to be used for the
% remainder of the code (based on USEPOD option), then it will replace the
% directory and file names of the velocity fields
if cadat.options.RUNPOD
    fprintf('\nRunning POD on data...\n')
    % Load in all velocity files, input needs to be a 4D matrix (x,y,z,t).
    % Note** This could mean a VERY BIG matrix that requires A LOT of RAM!
    % Be careful to ensure the processing computer has enough memory!
    %%% Load velocity file %%%%%%%%%%%%%%%%%%%%%%%%%%%%%%%%%%%%%%%%%%%%%%%%
    fprintf('Loading data...')
    iter = 1;
    prev_mark = 0;
    num_t = length(cadat.options.TS:cadat.options.Tskip:cadat.options.TE);
    for q = cadat.options.TS:cadat.options.Tskip:cadat.options.TE
        fp = load([cadat.DIR.velfiles,cadat.FILE.basename,num2str(q,'%05i'),'.mat']); %what;
change this
        % Get current velocities
        x = fp.x;
        y = fp.y;
        z = fp.z;
        u = fp.u;
        v = fp.v;
        w = fp.w;
        t = fp.t;

        % Place the velocities on a grid
        cu = zeros(size(velmask));
        cv = zeros(size(velmask));
        cw = zeros(size(velmask));
        for ptn = 1:1:length(x)
            [~,cind] = min(abs(maskX - x(ptn)));
```

```
        [~,rind] = min(abs(maskY - y(ptn)));
        [~,zind] = min(abs(maskZ - z(ptn)));

        % Put velocity in corresponding spatial location
        cu(rind,cind,zind) = u(ptn);
        cv(rind,cind,zind) = v(ptn);
        cw(rind,cind,zind) = w(ptn);
    end
    % Save all velocities into single array
    ua(:,:,:,iter) = cu;
    va(:,:,:,iter) = cv;
    wa(:,:,:,iter) = cw;
    ta(iter,1) = t;
    % Increment count
    iter = iter + 1;

    % Print the percent completed for steps of 10
    perc_complete = floor(100*iter/num_t);
    if (mod(perc_complete,10) == 0) && (perc_complete ~= prev_mark)
        fprintf(' %i%%',perc_complete)
        prev_mark = perc_complete;
    end
end
fprintf(' completed successfully')
%%% Run POD %%%%%%%%%%%%%%%%%%%%%%%%%%%%%%%%%%%%%%%%%%%%%%%%%%%%%%%%%%%%%%%%
fprintf('\nPerforming POD...')
[Us,Vs,Ws,mkp,D] = POD3(ua,va,wa,2);
fprintf('\nPOD completed successfully')
%%% Save POD files for each time step %%%%%%%%%%%%%%%%%%%%%%%%%%%%%%%%%%%%%
fprintf('\nSaving POD velocity files...')
% Convert x, y, z grids to lines
Vxl = reshape(Vx,[size(Vx,1)*size(Vx,2)*size(Vx,3),1]);
Vyl = reshape(Vy,[size(Vx,1)*size(Vx,2)*size(Vx,3),1]);
Vzl = reshape(Vz,[size(Vx,1)*size(Vx,2)*size(Vx,3),1]);

% Iterate through all time steps to save to mat and dat files
iter = 1;
prev_mark = 0;
for q = cadat.options.TS:cadat.options.Tskip:cadat.options.TE %cadat.options.TS
    % Get current velocity fields
    uc = Us(:,:,:,iter);
    vc = Vs(:,:,:,iter);
    wc = Ws(:,:,:,iter);

    % Mask to only include the velocity mask points
    uc( isnan(velmask) ) = NaN;
    vc( isnan(velmask) ) = NaN;
    wc( isnan(velmask) ) = NaN;

    % Convert velocities to line
    uc = reshape(uc,[size(uc,1)*size(uc,2)*size(uc,3),1]);
    vc = reshape(vc,[size(uc,1)*size(uc,2)*size(uc,3),1]);
    wc = reshape(wc,[size(uc,1)*size(uc,2)*size(uc,3),1]);

    % Keep only the real values (get rid of the NaNs)
    x = Vxl(~isnan(uc));
    y = Vyl(~isnan(uc));
    z = Vzl(~isnan(uc));
    u = uc(~isnan(uc));
    v = vc(~isnan(uc));
```

```
        w = wc(~isnan(uc));
        t = ta(iter,1);

        % Save mat file

save([cadat.DIR.podfiles,cadat.FILE.podname,num2str(q,'%05i'),'.mat'],'x','y','z','u','v','w',
't');

        % Save dat file
        % Initialize output file
        fid = fopen([cadat.DIR.podfiles,cadat.FILE.podname,num2str(q,'%05i'),'.dat'],'w');
        fprintf(fid,['TITLE = "',cadat.FILE.podname,num2str(q,'%05i'),'"']);
        fprintf(fid,'\nVARIABLES = "X", "Y", "Z", "U", "V", "W"\n');

        % Iterate through all points and write only those that are non-zero
        for zz = 1:1:length(x)
            cx = x(zz);
            cy = y(zz);
            cz = z(zz);
            cu = u(zz);
            cv = v(zz);
            cw = w(zz);
            fprintf(fid,'\n%.6f %.6f %.6f %.6f %.6f %.6f',cx,cy,cz,cu,cv,cw);
        end
        % Close dat file
        fclose(fid);

        % Increment count
        iter = iter + 1;

        % Print the percent completed for steps of 10
        perc_complete = floor(100*iter/num_t);
        if (mod(perc_complete,10) == 0) && (perc_complete ~= prev_mark)
            fprintf(' %i%%',perc_complete)
            prev_mark = perc_complete;
        end

    end
    fprintf('\n...completed successfully\n')
end

if cadat.options.USEPOD
    % Set directory and base name of velocity files to the pod ones
    cadat.DIR.velfiles = cadat.DIR.podfiles;
    cadat.FILE.basename = cadat.FILE.podname;
end
```

BIBLIOGRAPHY

[1] M. H. M Vlak *et al.*, "Prevalence of unruptured intracranial aneurysms, with emphasis on sex, age, comorbidity, country, and time period: a systematic review and meta-analysis," *Articles Lancet Neurol*, vol. 10, pp. 626–662, 2011, doi: 10.1016/S1474.

[2] M. T. Lawton and G. E. Vates, "Subarachnoid Hemorrhage," *New England Journal of Medicine*, vol. 377, no. 3, pp. 257–266, Jul. 2017, doi: 10.1056/NEJMcp1605827.

[3] H. Lantigua *et al.*, "Subarachnoid hemorrhage: Who dies, and why?," *Crit Care*, vol. 19, no. 1, Aug. 2015, doi: 10.1186/s13054-015-1036-0.

[4] E. S. Connolly *et al.*, "Guidelines for the management of aneurysmal subarachnoid hemorrhage: A guideline for healthcare professionals from the american heart association/american stroke association," *Stroke*, vol. 43, no. 6. pp. 1711–1737, Jun. 2012. doi: 10.1161/STR.0b013e3182587839.

[5] J. R. Cebral *et al.*, "Regional Mapping of Flow and Wall Characteristics of Intracranial Aneurysms," *Ann Biomed Eng*, vol. 44, no. 12, pp. 3553–3567, Dec. 2016, doi: 10.1007/s10439-016-1682-7.

[6] J. P. Broderick *et al.*, "Greater rupture risk for familial as compared to sporadic unruptured intracranial aneurysms," *Stroke*, vol. 40, no. 6, pp. 1952–1957, Jun. 2009, doi: 10.1161/STROKEAHA.108.542571.

[7] S. Dhar *et al.*, "Morphology parameters for intracranial aneurysm rupture risk assessment," *Neurosurgery*, vol. 63, no. 2, pp. 185–196, Aug. 2008, doi: 10.1227/01.NEU.0000316847.64140.81.

[8] J. Xiang *et al.*, "Hemodynamic-morphologic discriminants for intracranial aneurysm rupture," *Stroke*, vol. 42, no. 1, pp. 144–152, Jan. 2011, doi: 10.1161/STROKEAHA.110.592923.

[9] M. Raschi *et al.*, "CFD and PTV analysis of hemodynamics in a growing intracranialaneurysm," *Int J Numer Method Biomed Eng*, vol. 28, no. 2, pp. 214–228, Feb. 2012, doi: 10.1002/cnm.1459.

[10] P. Van Ooij, J. J. Schneiders, H. A. Marquering, C. B. Majoie, E. Van Bavel, and A. J. Nederveen, "3D cine phase-contrast MRI at 3T in intracranial aneurysms compared with patient-specific computational fluid dynamics," *American Journal of Neuroradiology*, vol. 34, no. 9, pp. 1785–1791, 2013, doi: 10.3174/ajnr.A3484.

[11] M. C. Brindise *et al.*, "Multi-modality cerebral aneurysm haemodynamic analysis: In vivo 4D flow MRI, in vitro volumetric particle velocimetry and in silico computational fluid dynamics," *J R Soc Interface*, vol. 16, no. 158, 2019, doi: 10.1098/rsif.2019.0465.

[12] M. C. Brindise *et al.*, "Patient-Specific Cerebral Aneurysm Hemodynamics: Comparison of in vitro Volumetric Particle Velocimetry, Computational Fluid Dynamics (CFD), and in vivo 4D Flow MRI."

[13] L. Boussel *et al.*, "Aneurysm growth occurs at region of low wall shear stress: Patient-specific correlation of hemodynamics and growth in a longitudinal study," *Stroke*, vol. 39, no. 11, pp. 2997–3002, Nov. 2008, doi: 10.1161/STROKEAHA.108.521617.

[14] Y. Zhang, L. Jing, Y. Zhang, J. Liu, and X. Yang, "Low wall shear stress is associated with the rupture of intracranial aneurysm with known rupture point: Case report and literature review," *BMC Neurol*, vol. 16, no. 1, Nov. 2016, doi: 10.1186/s12883-016-0759-0.

[15] G. Zhou, Y. Zhu, Y. Yin, M. Su, and M. Li, "Association of wall shear stress with intracranial aneurysm rupture: Systematic review and meta-analysis," *Scientific Reports*, vol. 7, no. 1. Nature Publishing Group, Dec. 01, 2017. doi: 10.1038/s41598-017-05886-w.

[16] B. Staarmann, M. Smith, and C. J. Prestigiacomo, "Shear stress and aneurysms: A review," *Neurosurg Focus*, vol. 47, no. 1, Jul. 2019, doi: 10.3171/2019.4.FOCUS19225.

[17] L. der Jou, D. H. Lee, H. Morsi, and M. E. Mawad, "Wall shear stress on ruptured and unruptured intracranial aneurysms at the internal carotid artery," *American Journal of Neuroradiology*, vol. 29, no. 9, pp. 1761–1767, Oct. 2008, doi: 10.3174/ajnr.A1180.

[18] J. R. Cebral, F. Mut, J. Weir, and C. M. Putman, "Association of hemodynamic characteristics and cerebral aneurysm rupture," *American Journal of Neuroradiology*, vol. 32, no. 2, pp. 264–270, Feb. 2011, doi: 10.3174/ajnr.A2274.

[19] J. R. Cebral, M. A. Castro, J. E. Burgess, R. S. Pergolizzi, M. J. Sheridan, and C. M. Putman, "Characterization of Cerebral Aneurysms for Assessing Risk of Rupture By Using Patient-Specific Computational Hemodynamics Models."

[20] J. R. Cebral, F. Mut, J. Weir, and C. Putman, "Quantitative characterization of the hemodynamic environment in ruptured and unruptured brain aneurysms," *American Journal of Neuroradiology*, vol. 32, no. 1, pp. 145–151, Jan. 2011, doi: 10.3174/ajnr.A2419.

[21] J. R. Cebral, F. Mut, J. Weir, and C. Putman, "Quantitative characterization of the hemodynamic environment in ruptured and unruptured brain aneurysms," *American Journal of Neuroradiology*, vol. 32, no. 1, pp. 145–151, Jan. 2011, doi: 10.3174/ajnr.A2419.

[22] R. P. Patel, "A note on fully developed turbulent flow down a circular pipe," *The Aeronautical Journal*, vol. 78, no. 758–759, pp. 93–97, 1974, doi: 10.1017/S0001924000036514.

[23] M. Raffel, C. E. Willert, F. Scarano, C. J. Kähler, S. T. Wereley, and J. Kompenhans, "Particle Image Velocimetry A Practical Guide Third Edition."

[24] M. C. Brindise, M. M. Busse, and P. P. Vlachos, "Density- and viscosity-matched Newtonian and non-Newtonian blood-analog solutions with PDMS refractive index," *Experiments in Fluids*, vol. 59, no. 11. Springer Verlag, Nov. 01, 2018. doi: 10.1007/s00348-018-2629-6.

[25] D. Schanz, S. Gesemann, and A. Schröder, "Shake-The-Box: Lagrangian particle tracking at high particle image densities," *Exp Fluids*, vol. 57, no. 5, May 2016, doi: 10.1007/s00348-016-2157-1.

[26] M. C. Brindise and P. P. Vlachos, "Proper orthogonal decomposition truncation method for data denoising and order reduction," *Exp Fluids*, vol. 58, no. 4, Apr. 2017, doi: 10.1007/s00348-017-2320-3.

[27] T. Yagi *et al.*, "Experimental insights into flow impingement in cerebral aneurysm by stereoscopic particle image velocimetry: Transition from a laminar regime," *J R Soc Interface*, vol. 10, no. 82, Apr. 2013, doi: 10.1098/rsif.2012.1031.

[28] H. Chen, D. Li, R. Bai, and X. Wang, "Comparison of swirling strengths derived from two- and three-dimensional velocity fields in channel flow," *AIP Adv*, vol. 8, no. 5, May 2018, doi: 10.1063/1.5023533.

[29] D. Katritsis, L. Kaiktsis, A. Chaniotis, J. Pantos, E. P. Efstathopoulos, and V. Marmarelis, "Wall Shear Stress: Theoretical Considerations and Methods of Measurement," *Prog Cardiovasc Dis*, vol. 49, no. 5, pp. 307–329, Mar. 2007, doi: 10.1016/J.PCAD.2006.11.001.

ACADEMIC VITA

Evan Lawler

EDUCATION

The Pennsylvania State University, University Park, PA
Bachelor of Science, Mechanical Engineering
Expected May 2023
Schreyer Honors College
Academic Awards: President's Freshman Award, Schreyer Academic Excellence Scholarship, Dean's List

TECHNICAL EXPERIENCE

The Boeing Company, *Manufacturing Engineering Intern* May 2022 to August 2022

- Performed Manufacturing Execution System updates to over 2,000 master plans spanning the CH-47, MH-47, V-22, and F-18 programs to conform plans according to composite process action team guidance.
- Worked extensively in a variety of Mission Critical, Enterprise Resource Planning [ERP] software including Integrated Product Management System [IPDMS], Manufacturing Execution System [MES], Shop Floor Management system [SFM].
- Collaborated with Manufacturing Engineers, Planners, and Supply Chain leaders to assign commodity codes to a wide variety of parts to drive weekly purchasing for new production aircraft.

Beta Star Life Science Equipment, *Mechanical Design Engineer Intern* May 2021 to August 2021

- Responsible for redesign of BSL-2+ steam sterilizers based on design specifications. Managed feedback loops between customers and fabricators to optimize the design effort of over $2,000,000 of product.

Fluidcom Research Lab*, Undergraduate Researcher* September 2021 to Present

- Directly collaborated with Principal Investigator to support research which combines experimental flow physics with image and signal processing to improve analysis methods and current clinical understanding of neuro- and cardiovascular disease, injury, function, and treatment.
- Worked as part of the team in developing a scientific rationale for assessing certain fluid mechanical properties that may better enable medical interventions for high-risk brain aneurysms.

LEADERSHIP AND INVOLVEMENT

Penn State College of Engineering, *Career Envoy* August 2022 to Present

- Engage with students during weekly meetings and assist with interview preparation and job searching.
- Collaborated with faculty and other envoys to brainstorm ways of improving process and services.

SKILLS/INTERESTS

Skills: SolidWorks, Draft Sight, G-Code, MATLAB, Microsoft Office Suite, Finite Element Analysis